Title
ωB97M-V: A combinatorially optimized, range-separated hybrid, meta-GGA density functional with VV10 nonlocal correlation

Journal
The Journal of Chemical Physics, 144(21)

ISSN
0021-9606

Authors
Mardirossian, Narbe
Head-Gordon, Martin

Publication Date
2016-06-07

DOI
10.1063/1.4952647

Peer reviewed

ωB97M-V: A combinatorially-optimized, range-separated hybrid, meta-GGA density functional with VV10 nonlocal correlation

Narbe Mardirossian[†] and Martin Head-Gordon[*,†]

†*Kenneth S. Pitzer Center for Theoretical Chemistry, Department of Chemistry, University of California, Berkeley, California 94720, USA*
‡*Chemical Sciences Division, Lawrence Berkeley National Laboratory, Berkeley, California 94720, USA*

E-mail: mhg@cchem.berkeley.edu

Abstract

A combinatorially-optimized, range-separated hybrid, meta-GGA density functional with VV10 nonlocal correlation is presented. The final 12-parameter functional form is selected from approximately 10 billion candidate fits that are trained on a training set of 870 data points and tested on a primary test set of 2965 data points. The resulting density functional, ωB97M-V, is further tested for transferability on a secondary test set of 1152 data points. For comparison, ωB97M-V is benchmarked against 10 leading density functionals including M06-2X, ωB97X-D, M08-HX, M11, ωM05-D, and ωB97X-V. Encouragingly, the overall performance of ωB97M-V on nearly 5000 data points clearly surpasses all of the tested density functionals. In order to facilitate the use of ωB97M-V, its basis set dependence and integration grid sensitivity are thoroughly assessed, and recommendations that take into account both efficiency and accuracy are provided.

1 Introduction

Density functional theory (DFT) is built on exact foundations,[1] but the exact functional, even if it were accessible, would likely be so complicated that it would give little practical advantage relative to the best wave function theories. The great achievement of functional development to date is the fact that very approximate functionals can provide useful levels of accuracy for many electronic structure problems in chemistry and condensed matter physics. The quest to obtain improved functionals that are computationally tractable continues in many research groups today, and this paper describes a promising effort in that direction.

The parameterization of empirical density functionals via linear least-squares fitting is perhaps the most widely-used method for functional development in the quantum chemistry community. Introduced by Axel Becke with the B97 density functional,[2] it relies on expanding inhomogeneity variables based on physically-relevant ingredients, such as the spin-density (ρ_σ), its gradient ($|\nabla\rho_\sigma|$), or the kinetic energy density ($\tau_\sigma = \sum_i^{occ.} |\nabla\psi_{i\sigma}|^2$), in one or more power series, whose coefficients are determined with the use of a training set of high-quality reference values.

Since 1997, at least 40 semi-empirical density functionals have been developed based on the concept introduced by B97. These functionals range from generalized gradient approximation (GGA) and nonseparable gradient approximation (NGA) functionals to meta-GGA

and meta-NGA functionals. GGAs, representing Rung 2 of Perdew's Jacob's Ladder,[3] usually depend on a single inhomogeneity variable that is a function of both ρ_σ and $|\nabla\rho_\sigma|$, while NGAs additionally depend on an inhomogeneity variable that is solely a function of ρ_σ. meta-GGAs (Rung 3) expand upon GGAs by including an additional dependence on an inhomogeneity variable that depends on ρ_σ and τ_σ, while meta-NGAs expand upon meta-GGAs in the same way that NGAs expand upon GGAs.

The inclusion of exact exchange, popularized in 1993 with the B3PW91 density functional,[4] has conventionally been of the global variety, meaning that the fraction of exact exchange is uniform for all interelectronic distances. More recently, these global hybrids have often been replaced by range-separated hybrid (RSH) functionals,[5] which have a fraction of short-range exact exchange that typically either smoothly increases to 1 (long-range-corrected) or smoothly decreases to 0 (long-range-screened).

Finally, since density functionals are unable to properly account for long-range correlation, most modern parameterizations simultaneously train a dispersion correction onto the local exchange-correlation functional. The simplest form for a dispersion correction is a damped, atom-atom potential (DFT-D) such as Grimme's DFT-D2 or DFT-D3 models.[6–8] A more rigorous treatment of dispersion is provided by nonlocal correlation (NLC) functionals such as VV10[9] and vdW-DF-2.[10] However, the most elaborate and computationally demanding choice for a dispersion correction is a post-Hartree–Fock correlation (post-HFC) method such as MP2, MP3, RPA, or CCSD.

In light of the above considerations, Figure 1 presents an alternate view of elements that can be combined to define most existing density functionals. The first element (**Local Exchange-Correlation**) pertains to the ingredients that constitute the local exchange-correlation functional, with the available choices mimicking the first three rungs of Jacob's Ladder. The second element (**Exact Exchange**) pertains to the optional use of exact exchange contributions to define hybrid functionals. Finally, the third element (**Dispersion Correction**) generally accounts for the optional treatment of long-range correlation by the approaches discussed above.

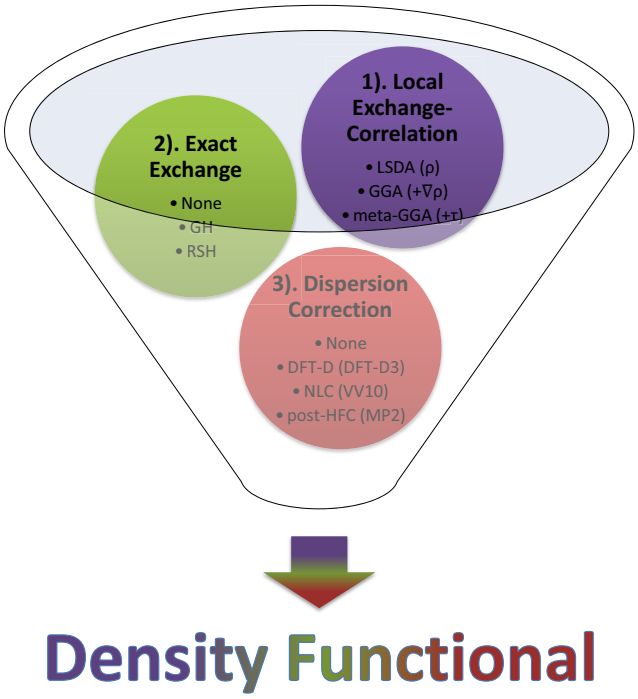

Figure 1: An alternate view of elements that can be combined to define most existing density functionals.

A selection of semi-empirical density functionals based on the B97 concept are listed below (dispersion-corrected functionals are underlined):

- **GGA Functionals**
  - **Local**: HCTH/93, HCTH/120, HCTH/147, HCTH/407, B97-D, SOGGA11[6,11–14]
  - **Global Hybrid**: B97-1, B97-2, B97-K, B97-3, SOGGA11-X[11,15–18]
  - **Range-Separated Hybrid**: ωB97, ωB97X, ωB97X-D, ωB97X-D3, ωB97X-V[19–22]
- **NGA Functionals**
  - **Local**: N12, GAM[23,24]
  - **Range-Separated Hybrid**: N12-SX[25]
- **meta-GGA Functionals**

- **Local**: τ-HCTH, M06-L, M11-L, B97M-V[26–29]
- **Global Hybrid**: τ-HCTHh, BMK, M05, M05-2X, M06, M06-2X, M06-HF, M08-HX, M08-SO[16,26,30–34]
- **Range-Separated Hybrid**: M11, ωM05-D, ωM06-D3[21,35,36]

• **meta-NGA Functionals**

- **Local**: MN12-L, MN15-L[37,38]
- **Range-Separated Hybrid**: MN12-SX[25]

The simplest form for the power series utilized in GGA functionals is

$$f(y) = \sum_{j=0}^{N} c_j y^j, \tag{1}$$

with y representing an inhomogeneity variable based on one of the aforementioned physically-relevant ingredients, and N representing the maximum truncation order for the summation. Conventionally, the value of N has either been chosen a priori or determined based on a "goodness-of-fit" to the training set. Smaller values of N can yield smoother and thus perhaps more transferable inhomogeneity correction factors, while larger values necessarily provide better fits to training data, whose transferability must subsequently be assessed.

The most general approach, however, is to choose a value for N and consider all possible combinations of the $N+1$ coefficients. This approach was explored several years ago,[39] resulting in the development of the ωB97X-V functional.[22] Using this combinatorial approach leads to a total of 2^{N+1}-1 fits, instead of just a handful. With a large number of candidate fits, the transferability of the fits can be assessed on a test set, allowing them to be ranked based on both their training set and test set performance. Furthermore, fits can be discarded based on undesirable physical characteristics or other relevant criteria.

By contrast with the one-dimensional power series characterizing a GGA density functional, the most general power series that can accommodate a meta-GGA density functional is two-dimensional:

$$f(x,y) = \sum_{i=0}^{N'} \sum_{j=0}^{N} c_{ij} x^i y^j. \tag{2}$$

In the spirit of the original B97 density functional, three components of the local exchange-correlation functional require parameterization: exchange, same-spin correlation, and opposite-spin correlation. With each component contributing $(N'+1)(N+1)$ coefficients, the total number of possible fits is $2^{3(N'+1)(N+1)}$-1. Setting N', the meta-GGA maximum truncation order, to 8, and N, the GGA maximum truncation order, to 4, brings the total number of possible combinations to an astounding 2^{135}-1$\approx 10^{41}$, a "functional genome" whose rank is approaching the square of Avogadro's number.

The development of the B97M-V density functional[29] was a first attempt at a partial search of the meta-GGA functional genome within the combinatorial optimization approach. Apart from the difficult issue of choosing appropriate weights for different sets of training and testing data, the main compromise made in the design of B97M-V was the choice to exclude exact exchange.

The goal of this paper is to improve upon B97M-V by revisiting the meta-GGA combinatorial search problem with the inclusion of exact exchange. The objective is to combinatorially design a range-separated hybrid, meta-GGA density functional which includes VV10 nonlocal correlation. It must be stressed that the combinatorial search performed to define B97M-V should not and will not be used in any direct way for this purpose. The addition of exact exchange means that different coefficients in Equation 2 will emerge as significant, perhaps apart from the few lowest-order terms. Unfortunately, the whole reason for adopting a combinatorial design approach is that it is impossible to anticipate *which* other terms will emerge as significant. Accordingly, it is a brand new search problem.

After describing the search process and its outcome, the functional which emerges as most

transferable (ωB97M-V) can then be compared to existing functionals. ωB97M-V will be compared against two functionals that were designed in a similar fashion (ωB97X-V and B97M-V), as well as some of the best alternative functionals from other groups, particularly those that include similar functional ingredients. However, no other existing functional yet combines precisely the same components as ωB97M-V.

A few of the issues that will be particularly interesting to examine are the following:

1. Comparing ωB97M-V against ωB97X-V will show the effect of meta-GGA local exchange-correlation against the corresponding GGA terms in an RSH containing VV10 nonlocal correlation.

2. Comparing ωB97M-V against B97M-V will indicate the value of exact exchange in combination with VV10 nonlocal correlation and meta-GGA local exchange-correlation.

3. Comparing against the best available semi-empirical hybrid meta-GGAs including M06-2X, M08-HX, M11, and ωM05-D will test the value of the combinatorial optimization strategy.

The hope is that within the limits of the functional form that has been chosen for optimization, the combinatorial design approach will permit the discovery of the most broadly accurate Rung 1-4 density functional to date.

2 Computational Details

Since several of the density functionals that appear in this paper contain both a local exchange-correlation functional and a nonlocal correlation functional, the integration grids used to evaluate these two components will be reported together, separated by a forward slash (local/nonlocal). Regarding the integration grid, the notation (x,y) indicates x radial shells with y angular grid points per shell.

The (99,590)/SG-1 grid was used for all of the datasets in the training, primary test, and secondary test sets, except AE18 and RG10. The (500,974)/(75,302) grid was used for both of these datasets. The def2-QZVPPD basis set was used for all of the datasets in the training, primary test, and secondary test sets, without counterpoise corrections.

For the basis set limit tests, the (99,590)/SG-1 grid was used, while 21 basis sets from 4 different families were tested: the cc-pVXZ and aug-cc-pVXZ (X=D,T,Q) Dunning basis sets,[40–42] the pc-X and aug-pc-X (X=0,1,2,3) Jensen basis sets,[43–45] the def2-SVP, def2-SVPD, and def2-XZVPP and def2-XZVPPD (X=T,Q) Karlsruhe basis sets,[46–50] and the 6-311++G(3df,3pd) Pople basis set. For the integration grid limit tests, the def2-QZVPPD basis set was used, while seven different grid combinations were tested: (250,974)/SG-1, (99,590)/SG-1, (99,302)/SG-1, (75,590)/SG-1, (75,302)/SG-1, (75,302)/SG-0, and SG-1/SG-0.[51,52]

All of the calculations were performed with a development version of Q-Chem 4.0.[53]

3 Datasets

A total of 84 existing datasets are employed in this work, containing 4987 data points (and requiring 5933 single-point calculations). 82 of these 84 datasets (AE18 and RG10 are excluded) are classified according to 8 categories (or datatypes): NCED (non-covalent dimers (easy)), NCEC (non-covalent clusters (easy)), NCD (non-covalent dimers (difficult)), IE (isomerization energies (easy)), ID (isomerization energies (difficult)), TCE (thermochemistry (easy)), TCD (thermochemistry (difficult)), and BH (barrier heights). The number of data points (and datasets) that are classified according to NCED, NCEC, NCD, IE, ID, TCE, TCD, and BH are 1744 (18), 243 (12), 92 (5), 755 (12), 155 (5), 947 (15), 258 (7), and 206 (8), respectively.

For purposes of functional development and testing, the datasets are divided into three categories. A training set is used to fit the parameters of each candidate functional in the combinatorial search, and then again to self-

consistently train the best candidate. A primary test set is used in conjunction with the training set to perform the combinatorial search, and identify the best candidate (details of this procedure are given in Section 5). Finally, a secondary test set is used to assess the final optimized functional. Detailed information about the training, primary test, and secondary test sets can be found in Table 1. The training set contains 870 data points overall, the primary test set contains 2965 data points overall, and the secondary test set contains 1152 data points overall. Thus, the training set constitutes only 17.5% of the entire database used to develop and assess ωB97M-V.

4 Theory

The complete functional form for ωB97M-V is given by Equations 3-5. The acronyms used in this section are: exchange-correlation (xc), exchange (x), correlation (c), short-range (sr), long-range (lr), meta-GGA (mGGA), same-spin (ss), opposite-spin (os), and nonlocal (nl).

$$E_{xc}^{\omega B97M-V} = E_{x}^{\omega B97M-V} + E_{c}^{\omega B97M-V} \tag{3}$$

$$E_{x}^{\omega B97M-V} = E_{x,sr}^{mGGA} + c_x E_{x,sr}^{exact} + E_{x,lr}^{exact} \tag{4}$$

$$E_{c}^{\omega B97M-V} = E_{c,ss}^{mGGA} + E_{c,os}^{mGGA} + E_{c,nl}^{VV10} \tag{5}$$

The local spin-density approximation (LSDA) for exchange can be expressed in terms of the first-order spinless reduced density matrix for an infinite uniform electron gas (UEG),

$$E_{x}^{LSDA} = -\frac{1}{2}\sum_{\sigma}^{\alpha,\beta}\int\int \frac{1}{s}\left|\rho_{\sigma}^{UEG}\right|^{2} d\mathbf{r}d\mathbf{s}, \tag{6}$$

$$\rho_{\sigma}^{UEG} = 3\rho_{\sigma}\left(\frac{\sin\left(k_{F\sigma}s\right) - k_{F\sigma}s\cos\left(k_{F\sigma}s\right)}{\left(k_{F\sigma}s\right)^{3}}\right), \tag{7}$$

where $\mathbf{s} = \mathbf{r}_1 - \mathbf{r}_2$, $\mathbf{r} = \frac{1}{2}\left(\mathbf{r}_1 + \mathbf{r}_2\right)$, and $k_{F\sigma} = \left(6\pi^2\rho_{\sigma}\right)^{1/3}$ is the spin-polarized Fermi wave vector. Integration of Equation 6 over $\mathbf{s}$ gives the well-known expression for the LSDA exchange energy in terms of the exchange energy density per unit volume,

$$E_{x}^{LSDA} = \sum_{\sigma}^{\alpha,\beta}\int e_{x,\sigma}^{UEG} d\mathbf{r}, \tag{8}$$

$$e_{x,\sigma}^{UEG} = -\frac{3}{2}\left(\frac{3}{4\pi}\right)^{1/3}\rho_{\sigma}^{4/3}, \tag{9}$$

Transforming E_{x}^{LSDA} to its short-range counterpart, $E_{x,sr}^{LSDA}$, is accomplished by replacing $\frac{1}{s}$ in Equation 6 with $\frac{\mathrm{erfc}(\omega s)}{s}$ and carrying out the same integration. The resulting SR-LSDA exchange functional,

$$E_{x,sr}^{LSDA} = \sum_{\sigma}^{\alpha,\beta}\int e_{x,\sigma}^{UEG} F_{x,\sigma} d\mathbf{r}, \tag{10}$$

is conveniently identical to its unattenuated counterpart, with the exception of a multiplicative factor,

$$\begin{aligned} F_{x,\sigma} = 1 - \frac{2}{3}a_{\sigma}\Bigg(2\sqrt{\pi}\mathrm{erf}\left(\frac{1}{a_{\sigma}}\right) - 3a_{\sigma} + \\ a_{\sigma}^{3} + \left(2a_{\sigma} - a_{\sigma}^{3}\right)\exp\left(-\frac{1}{a_{\sigma}^{2}}\right)\Bigg), \end{aligned} \tag{11}$$

where $a_{\sigma} = \frac{\omega}{k_{F\sigma}}$ and ω is a nonlinear parameter that controls the transition from local DFT exchange to nonlocal exact exchange with respect to interelectronic distance.

Accounting for inhomogeneities in the electron density is achieved by multiplying the integrand of the SR-LSDA exchange functional (Equation 10) by a power series inhomogeneity correction factor (ICF), g_x, resulting in the SR-mGGA exchange functional,

$$E_{x,sr}^{mGGA} = \sum_{\sigma}^{\alpha,\beta}\int e_{x,\sigma}^{UEG} F_{x,\sigma} g_x d\mathbf{r}, \tag{12}$$

$$g_x = \sum_{i}^{N'}\sum_{j}^{N} c_{x,ij} w_{x,\sigma}^{i} u_{x,\sigma}^{j}, \tag{13}$$

$$w_{x,\sigma} = \frac{t_{\sigma} - 1}{t_{\sigma} + 1}, \tag{14}$$

$$u_{x,\sigma} = \frac{\gamma_x s_{\sigma}^{2}}{1 + \gamma_x s_{\sigma}^{2}}, \tag{15}$$

where the variable, $w_{x,\sigma} \in [-1, 1]$, is a finite domain transformation of the dimensionless ratio of the UEG kinetic energy density to the exact kinetic energy density, $t_{\sigma} = \frac{\tau_{\sigma}^{UEG}}{\tau_{\sigma}}$, with $\tau_{\sigma}^{UEG} = \frac{3}{5}\left(6\pi^2\right)^{2/3}\rho_{\sigma}^{5/3}$, and the variable, $u_{x,\sigma} \in [0, 1]$, is a finite domain transformation of the dimensionless spin-density gradient, $s_{\sigma} = \frac{|\nabla\rho_{\sigma}|}{\rho_{\sigma}^{4/3}} \in [0, \infty)$. The linear DFT exchange parameters, $c_{x,ij}$, will be determined via least-

Table 1: Summary of the 84 datasets that comprise the training, primary test, and secondary test sets. The datatypes are explained in Section 3. The sixth column contains the root-mean-squares of the dataset reaction energies. PEC stands for potential energy curve, SR stands for single-reference, MR stands for multi-reference, Bz stands for benzene, Me stands for methane, and Py stands for pyridine.

Name	Set	Datatype	#	Description	ΔE (kcal/mol)	Ref.
A24	Train	NCED	24	Binding energies of small non-covalent complexes	2.65	54
DS14	Train	NCED	14	Binding energies of complexes containing divalent sulfur	3.70	55
HB15	Train	NCED	15	Binding energies of hydrogen-bonded dimers featuring ionic groups common in biomolecules	19.91	56
HSG	Train	NCED	21	Binding energies of small ligands interacting with protein receptors	6.63	57,58
NBC10	Train	NCED	184	PECs for BzBz (5), BzMe (1), MeMe (1), BzH_2S (1), and PyPy (2)	1.91	58–61
S22	Train	NCED	22	Binding energies of hydrogen- and dispersion-bonded non-covalent complexes	9.65	58,62
X40	Train	NCED	31	Binding energies of non-covalent interactions involving halogenated molecules	5.26	63
A21x12	PriTest	NCED	252	PECs for the 21 equilibrium complexes from A24	1.43	64
BzDC215	PriTest	NCED	215	PECs for benzene interacting with two rare-gas atoms and eight first- and second-row hydrides	1.81	65
HW30	PriTest	NCED	30	Binding energies of hydrocarbon-water dimers	2.34	66
NC15	PriTest	NCED	15	Binding energies of very small non-covalent complexes	0.95	67
S66	PriTest	NCED	66	Binding energies of non-covalent interactions found in organic molecules and biomolecules	6.88	68,69
S66x8	PriTest	NCED	528	PECs for the 66 complexes from S66x8	5.57	68
3B-69-DIM	SecTest	NCED	207	Binding energies of all relevant pairs of monomers from 3B-69-TRIM	5.87	70
AlkBind12	SecTest	NCED	12	Binding energies of saturated and unsaturated hydrocarbon dimers	3.14	71
CO2Nitrogen16	SecTest	NCED	16	Binding energies of CO_2 to molecular models of pyridinic N-doped graphene	3.84	72
HB49	SecTest	NCED	49	Binding energies of small- and medium-sized hydrogen-bonded systems	14.12	73–75
Ionic43	SecTest	NCED	43	Binding energies of anion-neutral, cation-neutral, and anion-cation dimers	69.94	76
H2O6Bind8	Train	NCEC	8	Binding energies of isomers of $(H_2O)_6$	46.96	77,78
HW6Cl	Train	NCEC	6	Binding energies of $Cl^-(H_2O)_n$ ($n = 1-6$)	57.71	77,78
HW6F	Train	NCEC	6	Binding energies of $F^-(H_2O)_n$ ($n = 1-6$)	81.42	77,78
FmH2O10	PriTest	NCEC	10	Binding energies of isomers of $F^-(H_2O)_{10}$	168.50	77,78
Shields38	PriTest	NCEC	38	Binding energies of $(H_2O)_n$ ($n = 2-10$)	51.54	79
SW49Bind345	PriTest	NCEC	31	Binding energies of isomers of $SO_4{}^{2-}(H_2O)_n$ ($n = 3-5$)	28.83	80
SW49Bind6	PriTest	NCEC	18	Binding energies of isomers of $SO_4{}^{2-}(H_2O)_6$	62.11	80
WATER27	PriTest	NCEC	23	Binding energies of neutral and charged water clusters	67.48	81,82
3B-69-TRIM	SecTest	NCEC	69	Binding energies of trimers, with three different orientations of 23 distinct molecular crystals	14.36	70
CE20	SecTest	NCEC	20	Binding energies of water, ammonia, and hydrogen fluoride clusters	30.21	83,84
H2O20Bind10	SecTest	NCEC	10	Binding energies of isomers of $(H_2O)_{20}$ (low-energy structures)	198.16	78
H2O20Bind4	SecTest	NCEC	4	Binding energies of isomers of $(H_2O)_{20}$ (dod, fc, fs, and es)	206.12	81,82,85,86
TA13	Train	NCD	13	Binding energies of dimers involving radicals	22.00	87
XB18	Train	NCD	8	Binding energies of small halogen-bonded dimers	5.23	88
Bauza30	PriTest	NCD	30	Binding energies of halogen-, chalcogen-, and pnicogen-bonded dimers	23.65	89,90
CT20	PriTest	NCD	20	Binding energies of charge-transfer complexes	1.07	91
XB51	PriTest	NCD	21	Binding energies of large halogen-bonded dimers	7.77	88
AlkIsomer11	Train	IE	11	Isomerization energies of $n = 4-8$ alkanes	1.81	92
Butanediol65	Train	IE	65	Isomerization energies of butane-1,4-diol	2.89	93
ACONF	PriTest	IE	15	Isomerization energies of alkane conformers	2.23	82,94
CYCONF	PriTest	IE	11	Isomerization energies of cysteine conformers	2.00	82,95
Pentane14	PriTest	IE	14	Isomerization energies of stationary points on the n-pentane torsional surface	6.53	96
SW49Rel345	PriTest	IE	31	Isomerization energies of $SO_4{}^{2-}(H_2O)_n$ ($n = 3-5$)	1.47	80
SW49Rel6	PriTest	IE	18	Isomerization energies of $SO_4{}^{2-}(H_2O)_6$	1.22	80
H2O16Rel5	SecTest	IE	5	Isomerization energies of $(H_2O)_{16}$ (boat and cage structures)	0.40	97
H2O20Rel10	SecTest	IE	10	Isomerization energies of $(H_2O)_{20}$ (low-energy structures)	2.62	78
H2O20Rel4	SecTest	IE	4	Isomerization energies of $(H_2O)_{20}$ (dod, fc, fs, and es)	5.68	81,82,85,86
Melatonin52	SecTest	IE	52	Isomerization energies of melatonin	5.54	98
YMPJ519	SecTest	IE	519	Isomerization energies of the proteinogenic amino acids	8.33	99
EIE22	Train	ID	22	Isomerization energies of enecarbonyls	4.97	100
Styrene45	Train	ID	45	Isomerization energies of C_8H_8	68.69	101
DIE60	PriTest	ID	60	Isomerization energies of reactions involving double-bond migration in conjugated dienes	5.06	102
ISOMERIZATION20	PriTest	ID	20	Isomerization energies	44.05	103
C20C24	SecTest	ID	8	Isomerization energies of the ground state structures of C_{20} and C_{24}	36.12	104
AlkAtom19	Train	TCE	19	$n = 1-8$ alkane atomization energies	1829.31	92
BDE99nonMR	Train	TCE	83	Bond dissociation energies (SR)	114.98	103
G21EA	Train	TCE	25	Adiabatic electron affinities of atoms and small molecules	40.86	82,105
G21IP	Train	TCE	36	Adiabatic ionization potentials of atoms and small molecules	265.35	82,105
TAE140nonMR	Train	TCE	124	Total atomization energies (SR)	381.05	103
AlkIsod14	PriTest	TCE	14	$n = 3-8$ alkane isodesmic reaction energies	10.35	92
BH76RC	PriTest	TCE	30	Reaction energies from HTBH38 and NHTBH38	30.44	82,106,107
EA13	PriTest	TCE	13	Adiabatic electron affinities	42.51	108
HAT707nonMR	PriTest	TCE	505	Heavy-atom transfer energies (SR)	74.79	103
IP13	PriTest	TCE	13	Adiabatic ionization potentials	256.24	108
NBPRC	PriTest	TCE	12	Reactions involving NH_3/BH_3 and PH_3/BH_3	30.52	82,109,110
SN13	PriTest	TCE	13	Nucleophilic substitution energies	25.67	103
BSR36	SecTest	TCE	36	Hydrocarbon bond separation reaction energies	20.06	110,111
HNBrBDE18	SecTest	TCE	18	Homolytic N–Br bond dissociation energies	56.95	112
WCPT6	SecTest	TCE	6	Tautomerization energies for water-catalyzed proton-transfer reactions	7.53	113
BDE99MR	PriTest	TCD	16	Bond dissociation energies (MR)	54.51	103
HAT707MR	PriTest	TCD	202	Heavy-atom transfer energies (MR)	83.41	103
TAE140MR	PriTest	TCD	16	Total atomization energies (MR)	147.20	103
PlatonicHD6	SecTest	TCD	6	Homodesmotic reactions involving platonic hydrocarbon cages, C_nH_n ($n = 4, 6, 8, 10, 12, 20$)	136.71	114
PlatonicID6	SecTest	TCD	6	Isodesmic reactions involving platonic hydrocarbon cages, C_nH_n ($n = 4, 6, 8, 10, 12, 20$)	96.19	114
PlatonicIG6	SecTest	TCD	6	Isogyric reactions involving platonic hydrocarbon cages, C_nH_n ($n = 4, 6, 8, 10, 12, 20$)	356.33	114
PlatonicTAE6	SecTest	TCD	6	Total atomization energies of platonic hydrocarbon cages, C_nH_n ($n = 4, 6, 8, 10, 12, 20$)	2539.27	114
BHPERI26	Train	BH	26	Barrier heights of pericyclic reactions	23.15	82,115
CRBH20	Train	BH	20	Barrier heights for cycloreversion of heterocyclic rings	46.40	116
DBH24	Train	BH	24	Diverse barrier heights	28.34	117,118
CR20	PriTest	BH	20	Cycloreversion reaction energies	22.31	119
HTBH38	PriTest	BH	38	Hydrogen transfer barrier heights	16.05	107
NHTBH38	PriTest	BH	38	Non-hydrogen transfer barrier heights	33.48	106
PX13	SecTest	BH	13	Barrier heights for proton exchange in water, ammonia, and hydrogen fluoride clusters	28.83	83,84
WCPT27	SecTest	BH	27	Barrier heights for water-catalyzed proton-transfer reactions	38.73	113
AE18	Train	-	18	Absolute atomic energies of hydrogen through argon	148,739.00	120
RG10	PriTest	-	569	PECs for the 10 rare-gas dimers involving helium through krypton	1.21	121

squares fitting to a training set in Section 5, while $\gamma_x = 0.004$ is a fixed nonlinear DFT exchange parameter that was fit to the Hartree–Fock exchange energies of 20 atoms in 1986 by Becke.[122]

Nonlocal exact exchange is introduced by splitting the conventional $\frac{1}{r}$ Coulomb operator into a short-range component ($E_{x,sr}^{exact}$) and a long-range component ($E_{x,lr}^{exact}$) with the $\frac{\mathrm{erfc}}{r}$ and $\frac{\mathrm{erf}}{r}$ Coulomb functions, respectively,

$$E_{x,sr}^{exact} = -\frac{1}{2}\sum_{\sigma}^{\alpha,\beta}\sum_{i,j}^{occ.}\int\int \psi_{i\sigma}^{*}(\mathbf{r}_1)\,\psi_{j\sigma}^{*}(\mathbf{r}_2)\,\frac{\mathrm{erfc}(\omega r_{12})}{r_{12}} \psi_{j\sigma}(\mathbf{r}_1)\,\psi_{i\sigma}(\mathbf{r}_2)\,d\mathbf{r}_1 d\mathbf{r}_2, \tag{16}$$

$$E_{x,lr}^{exact} = -\frac{1}{2}\sum_{\sigma}^{\alpha,\beta}\sum_{i,j}^{occ.}\int\int \psi_{i\sigma}^{*}(\mathbf{r}_1)\,\psi_{j\sigma}^{*}(\mathbf{r}_2)\,\frac{\mathrm{erf}(\omega r_{12})}{r_{12}} \psi_{j\sigma}(\mathbf{r}_1)\,\psi_{i\sigma}(\mathbf{r}_2)\,d\mathbf{r}_1 d\mathbf{r}_2, \tag{17}$$

where $\psi_{i\sigma}$ and $\psi_{j\sigma}$ are occupied Kohn–Sham spatial orbitals. Instead of setting the percentage of exact-exchange at $r = 0$ to zero, an optimizable parameter, c_x, controls the amount of short-range exact exchange.

Closed-form expressions for the correlation energy density per particle of an infinite uniform electron gas, ϵ_c^{UEG}, are only known for the low- and high-density limits of the paramagnetic and ferromagnetic cases. Using the Monte-Carlo data of Ceperley and Alder,[123] Perdew and Wang developed an analytic spin-compensated representation,[124] ϵ_c^{PW92}, for ϵ_c^{UEG}. Combined with the spin-polarization interpolation formula of Vosko, Wilk, and Nusair,[125] the spin-polarized PW92 correlation energy density per electron, ϵ_c^{PW92}, is the starting point for the correlation functional,

$$E_c^{LSDA} = \int \rho \epsilon_c^{PW92} d\mathbf{r}. \tag{18}$$

Using the spin decomposition technique of Stoll and coworkers,[126] the LSDA correlation energy is separated into same-spin and opposite-spin components,

$$E_{c,ss}^{LSDA} = \sum_{\sigma}^{\alpha,\beta}\int e_{c,\sigma\sigma}^{PW92} d\mathbf{r} = \int \rho_\alpha \epsilon_c^{PW92}(\rho_\alpha, 0)\,d\mathbf{r} + \int \rho_\beta \epsilon_c^{PW92}(0, \rho_\beta)\,d\mathbf{r}, \tag{19}$$

$$E_{c,os}^{LSDA} = \int e_{c,\alpha\beta}^{PW92} d\mathbf{r} = \int \rho \epsilon_c^{PW92} d\mathbf{r} - \int \rho_\alpha \epsilon_c^{PW92}(\rho_\alpha, 0)\,d\mathbf{r} - \int \rho_\beta \epsilon_c^{PW92}(0, \rho_\beta)\,d\mathbf{r}, \tag{20}$$

where $e_{c,\sigma\sigma}^{PW92}$ and $e_{c,\alpha\beta}^{PW92}$ are the PW92 same-spin and opposite-spin correlation energy densities per unit volume, respectively. Extending Equations 19 and 20 to account for inhomogeneities in the electron density is straightforward, since the approach used for the exchange functional can be utilized,

$$E_{c,ss}^{mGGA} = \sum_{\sigma}^{\alpha,\beta}\int e_{c,\sigma\sigma}^{PW92} g_{c,ss} d\mathbf{r}, \tag{21}$$

$$g_{c,ss} = \sum_{i}^{N'}\sum_{j}^{N} c_{css,ij} w_{c,\sigma\sigma}^{i} u_{c,\sigma\sigma}^{j}, \tag{22}$$

$$w_{c,\sigma\sigma} = \frac{t_\sigma - 1}{t_\sigma + 1}, \tag{23}$$

$$u_{c,\sigma\sigma} = \frac{\gamma_{c,ss} s_\sigma^2}{1 + \gamma_{c,ss} s_\sigma^2}, \tag{24}$$

$$E_{c,os}^{mGGA} = \int e_{c,\alpha\beta}^{PW92} g_{c,os} d\mathbf{r}, \tag{25}$$

$$g_{c,os} = \sum_{i}^{N'}\sum_{j}^{N} c_{cos,ij} w_{c,\alpha\beta}^{i} u_{c,\alpha\beta}^{j}, \tag{26}$$

$$w_{c,\alpha\beta} = \frac{t_{\alpha\beta} - 1}{t_{\alpha\beta} + 1}, \tag{27}$$

$$u_{c,\alpha\beta} = \frac{\gamma_{c,os} s_{\alpha\beta}^2}{1 + \gamma_{c,os} s_{\alpha\beta}^2}, \tag{28}$$

where $t_{\alpha\beta} = \frac{1}{2}(t_\alpha + t_\beta)$ and $s_{\alpha\beta}^2 = \frac{1}{2}\left(s_\alpha^2 + s_\beta^2\right)$. The linear DFT correlation parameters, $c_{css,ij}$ and $c_{cos,ij}$, will be determined via least-squares fitting to a training set in Section 5, while $\gamma_{c,ss} = 0.2$ and $\gamma_{c,os} = 0.006$ are nonlinear DFT correlation parameters that were fit to the correlation energies of neon and helium in 1997 by Becke.[2]

Nonlocal correlation is taken into account via the VV10 NLC functional,[9]

$$E_{c,nl}^{VV10} = \int \rho\left(\mathbf{r}\right)\left[\frac{1}{32}\left[\frac{3}{b^2}\right]^{3/4} + \frac{1}{2}\int \rho\left(\mathbf{r}'\right)\Phi\left(\mathbf{r},\mathbf{r}',\{b,C\}\right)d\mathbf{r}'\right]d\mathbf{r}, \tag{29}$$

where $\Phi\left(\mathbf{r},\mathbf{r}',\{b,C\}\right)$ is the nonlocal correlation kernel defined in Reference 9. The VV10 NLC functional contains two nonlinear parameters: b, which controls the short-range damping of the $1/r^6$ asymptote, and C, which controls the accuracy of the asymptotic C_6 coefficients.

5 Training

With a total of 3835 data points in the training and primary test sets, a three-dimensional nonlinear optimization of the parameters associated with range-separation (ω) and VV10 (b and C) is impractical. As a result, the values of ω=0.3, b=6, and C=0.01 that were optimized for ωB97X-V are taken without further investigation. Any inaccuracies in these parameters will be accounted for during the optimization of the linear parameters.

In order to generate the data that is needed to carry out the least-squares fits, it is necessary to choose an initial guess for the linear coefficients. As explained in Section 1, the value of N' (the maximum truncation order for w in Equations 13, 22, and 26) is set to 8 and the value of N (the maximum truncation order for u in Equations 13, 22, and 26) is set to 4. This results in 135 coefficients that arise from the local exchange-correlation functional. Additionally, the fraction of short-range exact exchange (c_x) from Equation 4 is the 136th coefficient.

For the 135 coefficients that arise due to the three power series ICFs, the most flexible initial guess is that of the SR-LSDA, where $c_{x,00}$=$c_{css,00}$=$c_{cos,00}$=1, and the remaining 132 coefficients are zero. For c_x, the most straightforward initial guess is zero. However, since the contribution from exact exchange is bound to constitute a large fraction of the total exchange-correlation energy, it is beneficial to pick a value for c_x that is as close to the final value as possible, in order to minimize discrepancies between the RMSDs that are generated using the initial guess, and the RMSDs of the final, self-consistently optimized functional. With the value of $c_x = 0.167$ from ωB97X-V serving as a guide, the initial guess for the fraction of short-range exact exchange is set to $c_x = 0.15$. Finally, the only constraint that is explicitly enforced is the UEG limit for exchange ($c_{x,00}$+c_x=1).

The fundamental equations that will be used throughout the least-squares fitting procedure are

$$W_{Tr}^{1/2} A \Delta x = W_{Tr}^{1/2} b \tag{30}$$

and

$$\Delta x = (A^T W_{Tr} A)^{-1} (A^T W_{Tr} b), \tag{31}$$

where $\Delta x = x_{i+1} - x_i$ is the change in the linear coefficients (length: 136), W_{Tr} is a diagonal matrix of training weights (dimensions: 3835 x 3835), $b = E_{ref} - E_i$ is the difference between the reference and initial guess energies (length: 3835), and $A = A(x_i)$ is the matrix of ICF contributions (dimensions: 3835 x 136). While the first three quantities are conceptually straightforward, it is worthwhile to further explain how to generate the A matrix.

A is most generally a (# of data points) × (# of linear parameters) matrix. As an example, the element $A_{7,23}$ corresponds to the contribution to the 7th data point from the 23rd linear parameter ($c_{x,42}$). Assuming that the seventh data point corresponds to the binding energy of the water dimer from the S22 dataset, computing $A_{7,23}$ requires calculating the following quantity,

$$\sum_{\sigma}^{\alpha,\beta} \int e_{x,\sigma}^{UEG} F_{x,\sigma} w_{x,\sigma}^4 u_{x,\sigma}^2 d\mathbf{r}, \tag{32}$$

for the water dimer and both of its monomers, and computing the associated contribution to the binding energy. In this work, the A matrix is computed twice: once with the (99,590)/SG-1 grid and once with the (250,974)/SG-1 grid (the (500,974)/(75,302) grid is always used for AE18 and RG10). The rationale for computing A in two different grids will be explained when the filtering procedure is discussed. Unless otherwise specified, terms from Equations 30 and 31 that appear henceforth are computed with the (250,974)/SG-1 grid. To refer to the A ma-

trix computed in the (99,590)/SG-1 grid, the following notation will be used: $A^{(99,590)}$.

Since the optimization procedure involves both a training set (for determining the values of the coefficients) and a primary test set (for assessing the transferability of the resulting coefficients), a measure of the overall performance of the fits is necessary for ranking them. For this purpose, the total weighted root-mean-square-deviation (WRMSD),

$$WRMSD_{Total} = \sqrt{\frac{\mathrm{diag}\,(W) \cdot (A\Delta x - b)^2}{\#_{Total}}}, \qquad (33)$$

is used, where W is a diagonal matrix of training and primary test set weights (dimensions: 3835 x 3835). The diagonals of W and W_{Tr} are identical for the elements that belong to the training set, while W_{Tr} contains zeros for the elements that belong to the primary test set.

The weighting scheme used for ωB97M-V is considerably different than that used for B97M-V. Initially, each data point is given a weight that corresponds to the inverse of the product of the number of data points in the associated dataset and the root-mean-square of the reaction energies in the associated dataset. These values can be found in the fourth and sixth columns of Table 1, respectively. Within each of the datatypes, the weights are normalized by dividing by the smallest weight, and then exponentiated such that they lie between 1 and 2. For the determination of the weights only, the NCED and NCEC datatypes are consolidated into a single datatype, NCE, giving a total of seven datatypes. Furthermore, AE18 is included in the TCE datatype in order to receive a weight. Finally, each of the seven datatypes get a multiplicative weight based on intuition: 0.1 for TCD, 1 for TCE, 10 for NCD, ID, and BH, and 100 for NCE and IE. As RG10 does not belong to a datatype, it gets a weight of 10000. At this point, all of the datapoints (besides those in RG10) have a weight between 0.1 and 200. In order to promote transferability, the datasets in the primary test set get another multiplicative weight of 2.

Following the initial setup described above, the search for the optimal least-squares fit can proceed. Applying the single UEG constraint to the initial parameter space of 136 brings the total number of linearly independent parameters to 135. With the available computing resources (a 64-core node), the maximum number of fits that can be performed in a single day is around two billion. Therefore 135C5=346,700,277, which returns only 5-parameter fits, is the largest calculation that can be performed in a single day using all 135 parameters (since 135C6=7,511,839,335). In order to explore fits with more parameters, it is necessary to either consider different truncations of the parameter space or compulsorily-select commonly-occurring parameters. The first option reduces the value of n (from nCk), allowing for larger values of k. For example, the binomial coefficients 135C5 and 82C6 are both similar in value, yet the latter allows the exploration of 6-parameter fits. The second option requires F parameters to be compulsorily-selected (or frozen), allowing for the exploration of (n-F)Ck (k+F)-parameter fits. For example, if the results from 135C5 indicate that $c_{x,01}$ is the most important parameter, a possible next step would be to freeze $c_{x,01}$ (not its value but simply its inclusion in all successive fits) and explore the results of 134C5 with $c_{x,01}$ frozen, giving 6-parameter fits.

For the optimization of the functional at hand, a combination of these two options is utilized. While the meta-GGA parameter space described thus far contains 135 linearly independent parameters, its GGA subset contains only 15, which amounts to 2^{15}-1=32767 total possible fits. The GGA parameter space is fully searchable and the recent ωB97X-V density functional was developed within this subspace. Since ωB97X-V has seven linear parameters, it is plausible to assume that the minimum number of linear parameters necessary to parameterize a functional within the meta-GGA parameter space is seven. Thus, the initial parameter space of 135 should be truncated such that 7-parameter fits are possible without freezing. After considering a multitude of different truncations, a parameter space designated as 2I6I6I is selected. This includes variables up to second order individually in w and u for ex-

change and up to sixth order individually in w and u for same-spin and opposite-spin correlation. With 9 coefficients from exchange, 35 coefficients from same-spin correlation, 35 coefficients from opposite-spin correlation, an additional coefficient from short-range exact exchange, and a single constraint, the 2I6I6I designation reduces the parameter space from 135 to 79.

Although the 2I6I6I designation reduces the parameter space substantially, the largest calculation that is possible is still only 79C7=2,898,753,715. Thus, only up to 7-parameter fits can be explored. In order to advance past seven, it is necessary to compulsorily-select commonly-occurring parameters. The process of selecting the parameter that will be frozen involves a series of steps. First, from all of the 7-parameter fits resulting from the 79C7 optimization, the top 100,000 (ranked by total WRMSD) are saved and filtered twice. The first set of filters deals with the physical characteristics of the fits:

- $|x_{i+1}| \leq 25$
- $0 \leq g_x \leq 2.273$
- $-10 \leq g_{c,ss} \leq 10$
- $-10 \leq g_{c,os} \leq 10$
- $(E_i - E_i^{(99,590)}) + (A - A^{(99,590)})\Delta x \leq 0.015$ kcal/mol

Of the conditions listed above, the first ensures that the coefficients are small, the second ensures that the exchange functional obeys the local Lieb-Oxford bound *and* that all contributions to exchange are negative, the third and fourth ensure that the correlation functionals are well-behaved, and the last ensures that interaction energy errors attributed to the integration grid are no larger than 0.015 kcal/mol.

Following the first set of filters, at most 1000 of the remaining fits are passed through a second filter, which deals with the accuracy of the fits for predicting equilibrium bond lengths for non-covalent interactions. The BzDC215, NBC10, S66x8, and RG10 datasets are utilized to this effect. In total, these four datasets contain 96 PECs, with BzDC215, NBC10, and RG10 each having 10, and S66x8 having 66. However, the benzene-neon dimer PEC from BzDC215 is removed because of severe integration grid issues. The remaining 95 PECs are interpolated and the equilibrium bond lengths are evaluated for all of the fits that pass through the first filter. Only fits that have an RMSD of less than 0.03 Å are allowed through the second filter.

Finally, the surviving fits are analyzed in order to determine the coefficient that is most commonly used. This coefficient is then compulsorily-selected in the next set of least-squares fits in order to allow for the exploration of 8-parameter fits. This procedure was repeated until a total of eight parameters were frozen ($c_{x,01}$, $c_{x,10}$, $c_{css,10}$, $c_{css,20}$, $c_{cos,20}$, $c_{css,00}$, $c_{cos,10}$, $c_{cos,21}$). The progression from the 7-parameter fits to the 15-parameter fits can be tracked in Table 2.

Due to the nonlinear nature of the self-consistent field method, the A matrix changes with every update to the parameters (since $A = A(x_i)$), and it is very likely that the A matrix that is constructed from the initial guess will be vastly different from the last A matrix that will be used to finalize the parameters. Furthermore, the larger the difference between the starting and the ending point, the higher the chance that the initial RMSDs will differ significantly from the RMSDs of the final functional. In fact, this phenomenon was first encountered during the development of the B97M-V density functional and was bypassed by updating the initial guess with a better guess formed by the first nine parameters that were frozen. Since this methodology worked well during the development of B97M-V, it is utilized in the present work. Thus, the eight parameters shown in the first column of Table 2 ("Best 8") are used to update the SR-LSDA+VV10 initial guess.

With the updated guess, the A matrix is computed with both the (99,590)/SG-1 and (250,974)/SG-1 grids and the same procedure outlined above is followed. However, no additional parameters need to be frozen, since with eight parameters already frozen, it is trivial

Table 2: Progression from the 7-parameter fits to the 15-parameter fits based on the SR-LSDA+VV10 initial guess. The first column indicates the additional coefficient that is frozen (compulsorily-selected) in order to achieve the associated set of fits. The second column contains the total number of least-squares fits that are performed, of which only the top 100,000 (ranked by total WRMSD) are analyzed. The fourth column indicates the number of fits (of 100,000) that remain after the first filter is applied. The fifth column indicates the number of fits (of at most 1000) from the previous column that remain after the second filter is applied. Finally, the last column indicates the coefficient that is most commonly utilized in the surviving fits (shown in Column 5).

Frozen	# of Initial Fits	# (Fitted)	Filter 1	Filter 2	Common
–	2,898,753,715	7	3342	413	$c_{x,01}$
$c_{x,01}$	2,641,902,120	8	1476	454	$c_{x,10}$
$c_{x,10}$	2,404,808,340	9	2806	623	$c_{css,10}$
$c_{css,10}$	2,186,189,400	10	7144	764	$c_{css,20}$
$c_{css,20}$	1,984,829,850	11	18021	591	$c_{cos,20}$
$c_{cos,20}$	1,799,579,064	12	6531	469	$c_{css,00}$
$c_{css,00}$	1,629,348,612	13	2985	696	$c_{cos,10}$
$c_{cos,10}$	1,473,109,704	14	1868	726	$c_{cos,21}$
$c_{cos,21}$	1,329,890,705	15	120	101	$c_{cos,60}$

to explore 9- through 15-parameter fits (71C1 through 71C7). However, both sets of filters are still applied. Beginning with the 9-parameter fits, an additional parameter is accepted only if it improves the total WRMSD by more than 0.05 kcal/mol (a protocol which was successfully utilized during the exploration of the GGA subspace[39]). Consequently, a 12-parameter fit emerges as the optimal fit and is self-consistently optimized. The progression of the minimum total WRMSDs from the 9- to 15-parameters fits is: {–, 5.04, 3.52, **3.46**, 3.44, 3.42, 3.39}. The WRMSDs corresponding to the least-squares fits from the SR-LSDA+VV10 initial guess and the "Best 8" updated guess are shown in Figure 2 in red and blue, respectively. The smallest WRMSD for a given number of linear parameters is displayed only for the "Best 8" data. The WRMSD of the least-squares fit that corresponds to ωB97M-V is boxed.

Table 3: Linear parameters from the beginning of all six cycles of the self-consistent optimization of ωB97M-V. The "Best 8" column refers to the freezing of eight commonly-occurring parameters. The nonlinear parameters that are taken from previous studies[2,22,122] are γ_x=0.004, $\gamma_{c,ss}$=0.2, $\gamma_{c,os}$=0.006, ω=0.3, b=6, and C=0.01.

Parameter	1	Best 8	3	4	5	6 (Final)
$c_{x,00}$	0.85	0.85	0.85	0.85	0.85	0.85
$c_{x,10}$	0	-0.097	0.265	0.259	0.259	0.259
$c_{x,01}$	0	0.789	1.014	1.007	1.007	1.007
$c_{css,00}$	1	0.216	0.457	0.443	0.443	0.443
$c_{css,10}$	0	-2.496	-4.868	-4.55	-4.536	-4.535
$c_{css,20}$	0	-0.816	-3.401	-3.391	-3.39	-3.39
$c_{css,43}$	0	0	4.107	4.267	4.278	4.278
$c_{css,04}$	0	0	-1.533	-1.438	-1.437	-1.437
$c_{cos,00}$	1	1	1	1	1	1
$c_{cos,10}$	0	3.13	1.573	1.372	1.359	1.358
$c_{cos,20}$	0	1.736	3.002	2.931	2.925	2.924
$c_{cos,60}$	0	0	-1.736	-1.419	-1.392	-1.39
$c_{cos,21}$	0	-1.591	-8.241	-8.776	-8.81	-8.812
$c_{cos,61}$	0	0	8.582	9.113	9.141	9.142
c_x	0.15	0.15	0.15	0.15	0.15	0.15

Including the initial cycle (Cycle 1) with the unoptimized ωB97M-V density functional as well as the "Best 8" cycle, the self-consistent optimization of ωB97M-V required six cycles. The final parameters of ωB97M-V can be found in the last column of Table 3, and Figure 3

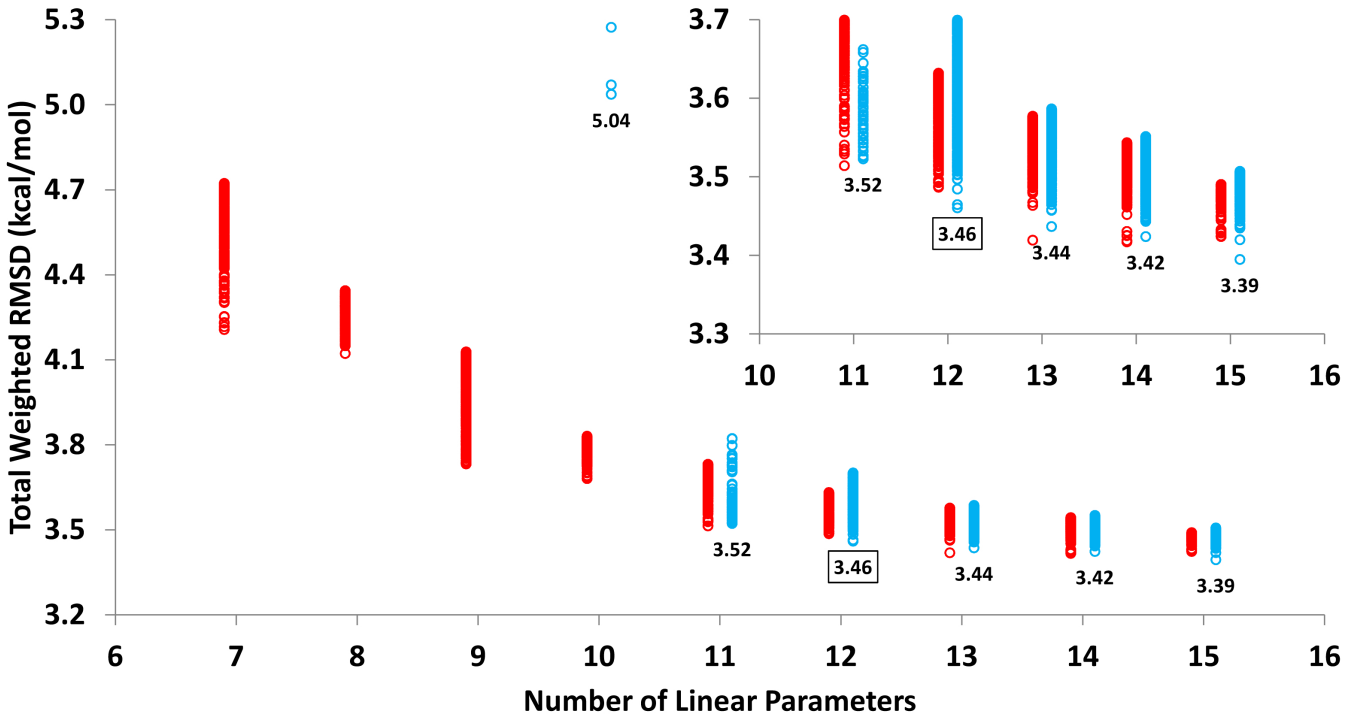

Figure 2: WRMSDs corresponding to the least-squares fits from the SR-LSDA+VV10 initial guess (red) and the "Best 8" updated guess (blue). The smallest WRMSD for a given number of linear parameters is displayed only for the "Best 8" data. The WRMSD of the least-squares fit that corresponds to ωB97M-V is boxed.

shows the exchange, same-spin correlation, and opposite-spin correlation ICF plots for ωB97M-V (bottom). In addition, it displays the ICFs for the SR-LSDA+VV10 initial guess (top) and the "Best 8" updated guess (middle). The final ICFs of ωB97M-V are smooth and well-behaved, with the maximum value of the exchange ICF (2.116) lying well under the Lieb-Oxford bound (2.273). The lower and upper bounds of all three ICFs are:

- $0.591 \leq g_x \leq 2.116$
- $-7.482 \leq g_{c,ss} \leq 4.429$
- $-1.957 \leq g_{c,os} \leq 4.222$

The four parameters that are chosen in addition to the "Best 8" are $c_{css,43}$, $c_{css,04}$, $c_{cos,60}$, and $c_{cos,61}$. Interestingly, the chosen fit does not optimize the value of short-range exact exchange away from $c_x = 0.15$.

6 Results

In order to verify that ωB97M-V is a broadly accurate density functional, it is necessary to compare it to existing density functionals. Thus, 10 exemplary density functionals are selected for comparison to ωB97M-V across the nearly 5000 data points in the training, primary test, and secondary test sets. Furthermore, all 11 functionals are benchmarked on 90 potential energy curves in order to assess equilibrium binding energies and bond lengths. Details for the 10 density functionals selected for comparison to ωB97M-V are shown in Table 4.

6.1 Overall Test Set Performance

Since the training, primary test, and secondary test sets contain 84 datasets overall, it is easier to obtain a general idea of the performance of ωB97M-V by first considering the eight datatypes defined in Section 3. However, in order to make the comparison as unbiased

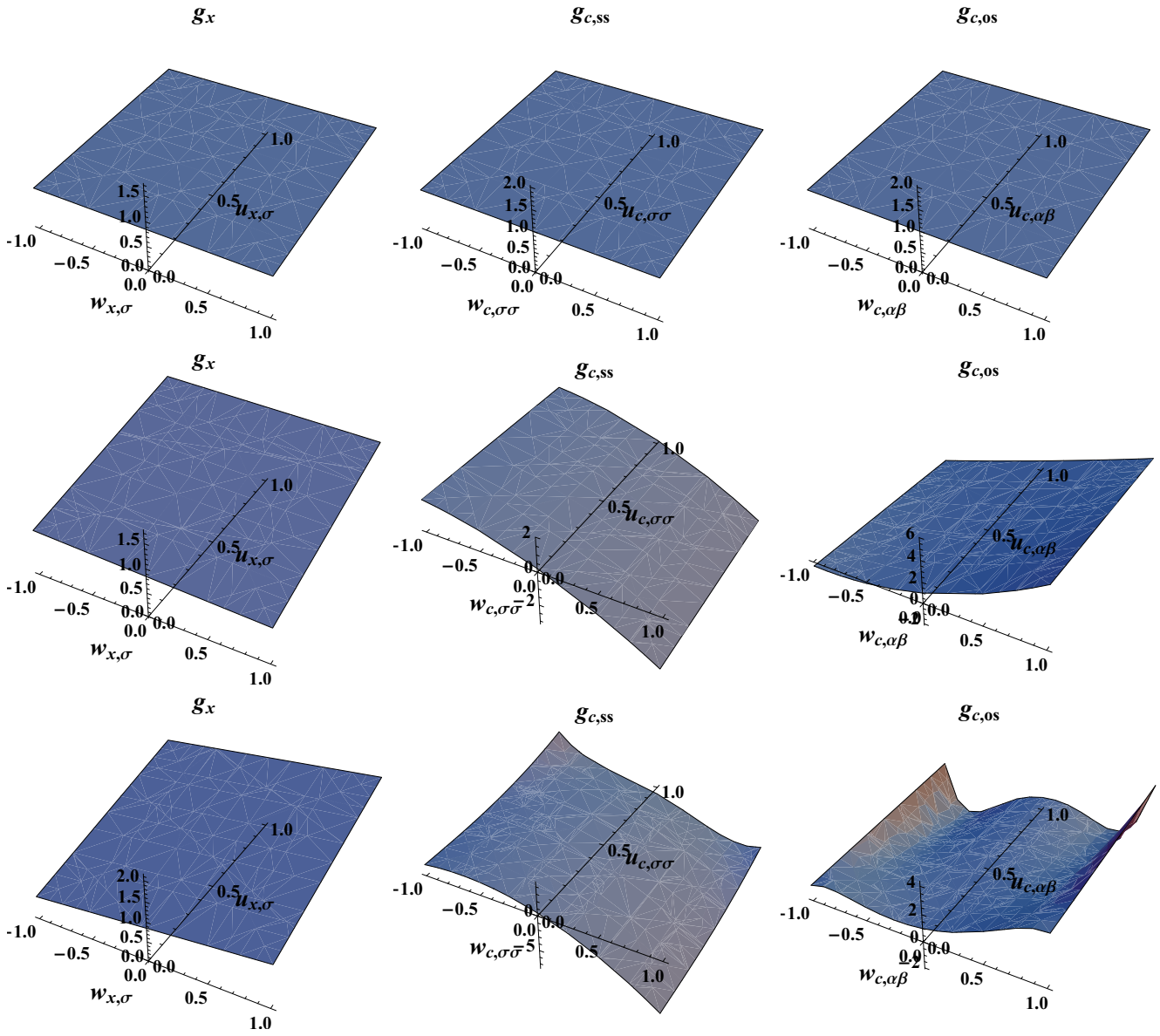

Figure 3: Exchange, same-spin correlation, and opposite-spin correlation inhomogeneity correction factor plots for the ωB97M-V density functional (bottom). In addition, the ICFs for the SR-LSDA+VV10 initial guess (top) and the "Best 8" updated guess (middle) are included for comparison.

Table 4: Details for the 10 exemplary functionals chosen for comparison to ωB97M-V. L stands for local, GH stands for global hybrid, and RSH stands for range-separated hybrid. The second column lists the number of parameters that were optimized on a training set for the given functional. The third column lists the percentage of exact exchange, c_x, as well as the value for ω in parentheses, if applicable. The column labeled UEG indicates whether or not the uniform electron gas limits were satisfied.

Functional	# (Fitted)	c_x (ω)	Class	Rung	UEG	Ref.
B97-D3(BJ)	12	0	L GGA DFT-D3(BJ)	2	No	6–8
B97M-V	12	0	L meta-GGA VV10	3	Yes	29
ωB97X-V	10	16.7-100 (0.3)	RSH GGA VV10	4	No	22
ωB97M-V	12	15-100 (0.3)	RSH meta-GGA VV10	4	No	–
ωB97X-D	15	22.2-100 (0.2)	RSH GGA CHG	4	Yes	20
ωM05-D	21	37.0-100 (0.2)	RSH meta-GGA CHG	4	Yes	36
M06-2X	29	54	GH meta-GGA	4	Yes	32
M08-HX	47	52.23	GH meta-GGA	4	Yes	34
M11	40	42.8-100 (0.25)	RSH meta-GGA	4	Yes	35
M06-L	34	0	L meta-GGA	3	Yes	27
MN15-L	58	0	L meta-NGA	3	No	38

as possible, only the data points from the primary and secondary test sets (henceforth referred to as the test set) are considered. Furthermore, since RG10 does not belong to any of the datatypes, it is excluded from this analysis. The total number of data points and datasets considered in Figure 4 are 3548 and 58, respectively.

Beginning with the NCED datatype, the functional with the best performance is ωB97M-V, with an RMSD of 0.18 kcal/mol. The next best functionals are ωB97X-V and B97M-V, both with RMSDs of 0.23 kcal/mol. Thus, the test set performance of ωB97M-V for over 1400 non-covalent dimer binding energies is at least 25% better than that of both of its predecessors. Besides the VV10-containing functionals, ωB97X-D and ωM05-D perform similarly, both with RMSDs of 0.38 kcal/mol, followed by M06-2X and B97-D3(BJ), which have RMSDs of 0.42 and 0.44 kcal/mol, respectively. The remaining functionals (M06-L, M08-HX, M11, and MN15-L) perform more poorly, with MN15-L being by far the poorest.

Moving on to the 223 non-covalent cluster binding energies in the test set with the NCEC datatype, the best performance is once again reserved for ωB97M-V, which has an RMSD of 0.50 kcal/mol. The next best functional (ωB97X-V) is about 30% worse, with an RMSD of 0.66 kcal/mol. Only two other functionals have RMSDs under or around 1 kcal/mol: B97M-V and ωB97X-D.

The NCD datatype contains non-covalent dimer binding energies that are susceptible to self-interaction error. Thus, local functionals should perform significantly worse than hybrid functionals, while hybrid functionals with a large fraction of exact exchange should perform best. Accordingly, the density functionals with the largest RMSDs across the 71 data points in the test set are the local ones, with RMSDs between 1.35 and 1.8 kcal/mol. Surprisingly, the best density functional is ωB97M-V, with an RMSD of 0.80 kcal/mol, just ahead of ωM05-D, which has 2.5 times more short-range exact exchange. M08-HX, M06-2X, and ωB97X-V are also close behind with RMSDs around 0.95 kcal/mol.

The test set contains a total of 679 isomerization energies, ranging from alkane conformers to amino acid conformers. The three functionals with the best performance for the IE data points in the test set are B97M-V, ωB97X-V, and ωB97M-V, with RMSDs slightly under 0.30 kcal/mol. The next best functionals are M06-2X (0.52 kcal/mol) and ωM05-D (0.54 kcal/mol), while five of the remaining six functionals (M08-HX, ωB97X-D, M06-L, M11, and B97-D3(BJ)) have RMSDs between 0.6 and 0.8 kcal/mol.

The ID datatype contains isomerization energies that are sensitive to self-interaction error. As with the NCD category, the local functionals exhibit the worst performance across the 88 data points in the test set, with RMSDs larger than 7.9 kcal/mol. From the hybrid functionals, ωB97X-V and ωB97M-V perform almost indistinguishably, with RMSDs of around 2.3 kcal/mol, while ωB97X-D performs about 65% worse, with an RMSD of 3.84 kcal/mol. The other hybrids have RMSDs that are 2 to 3 times larger than that of ωB97M-V.

The 660 TCE data points in the test set include heavy-atom transfer energies, homolytic bond dissociation energies, as well as isodesmic reaction energies. ωB97M-V is the best-

performing functional, with an RMSD of 2.45 kcal/mol. The next best functionals, M06-2X and ωM05-D, perform more than 30% worse, with RMSDs of 3.17 and 3.28 kcal/mol, respectively. The remaining four hybrids (M08-HX, M11, ωB97X-V, and ωB97X-D) perform comparably and have RMSDs around 3.6 kcal/mol. The best local functionals are B97M-V (3.59 kcal/mol) and MN15-L (3.95 kcal/mol), both performing significantly better than M06-L (5.26 kcal/mol).

Of the 258 TCD data points in the test set, 234 are multi-reference atomization energies, bond dissociation energies, and heavy-atom transfer energies from the W4-11 database, while 24 are atomization energies and homodesmotic, isodesmic, and isogyric reactions from the Platonic24 dataset. While the first grouping should be a major challenge for hybrid functionals, the second grouping should present difficulties for local functionals. The best-performing density functional is a hybrid (ωB97M-V with an RMSD of 4.30 kcal/mol), followed by a local functional (B97M-V with an RMSD of 4.82 kcal/mol). While ωB97X-V comes in third with an RMSD of 5.01 kcal/mol, the next best functionals are ωB97X-D and ωM05-D, with RMSDs of 5.79 and 5.87 kcal/mol, respectively. M06-2X performs about 65% worse than ωB97M-V, while M08-HX performs almost two times worse. The second-best local functional is B97-D3(BJ), with an RMSD (7.92 kcal/mol) that significantly improves over M06-L (12.97 kcal/mol).

Finally, the BH datatype contains five test datasets (136 data points), two of which (HTBH38 and NHTBH38) are found in the Minnesota density functional training sets. Nevertheless, ωB97M-V, with an RMSD of 1.80 kcal/mol, has the smallest RMSD out of the 11 benchmarked functionals, followed by M08-HX, which performs only slightly worse. Surprisingly, M06-2X is only fifth best, with an RMSD of 2.97 kcal/mol, followed closely by M11 (3.18 kcal/mol) and distantly by ωM05-D (4.11 kcal/mol). From the local functionals, B97M-V performs the best, with an RMSD of 3.95 kcal/mol, followed by MN15-L, which has an RMSD of 4.93 kcal/mol. M06-L performs about 25% worse than MN15-L, while the worst functional overall is B97-D3(BJ), with an RMSD of 7.85 kcal/mol.

Overall, the performance of ωB97M-V across 3548 test data points is very encouraging. Across the eight datatypes, ωB97M-V performs significantly better than the next best functional for four of the datatypes (NCED, NCEC, TCE, TCD), is indistinguishable from the next best functional for two of the datatypes (NCD and BH), and is indistinguishable from the best functional for the two remaining datatypes (IE and ID). It is worth noting that the size of the test set (3548 data points) used to validate ωB97M-V is more than 7 times larger than the entire 2015A Minnesota database used to train and test the latest MN15-L functional. Furthermore, of the 4987 total data points in the training, primary test, and secondary test sets, only 870 data points are used for training, while the other 82.5% are used for testing. Thus, the transferability of ωB97M-V is satisfactorily demonstrated with the results documented thus far.

6.2 Results for Individual Datasets

Figures 5, 6, and 7 contain RMSDs for datasets in the training, primary test, and secondary test sets, respectively. Although there are 84 datasets in total, the AE18 and RG10 datasets from the training and primary test sets are excluded. The performance of ωB97M-V on the training datasets will be discussed very briefly, since it is bad scientific practice to compare the performance of a semi-empirical density functional to that of existing functionals using its own training set.

One training result worth mentioning is that across the 124 atomization energies in the TAE140nonMR dataset,[103] ωB97M-V affords an RMSD of 2.23 kcal/mol, which significantly improves over ωB97X-V (2.95 kcal/mol) and B97M-V (3.89 kcal/mol). This shows the improvement that is possible by including exact exchange, nonlocal correlation, as well as meta-GGA local contributions, since TAE140nonMR was included in the training set of all three functionals.

Datatype	B97-D3(BJ)	B97M-V	ωB97X-V	ωB97M-V	ωB97X-D	ωM05-D	M06-2X	M08-HX	M11	M06-L	MN15-L
NCEDTest	0.44	0.23	0.23	0.18	0.38	0.38	0.42	0.57	0.61	0.54	1.39
NCECTest	4.91	0.99	0.66	0.50	1.03	1.82	2.48	1.73	2.92	2.27	13.20
NCDTest	1.80	1.45	0.97	0.80	1.10	0.82	0.94	0.93	1.32	1.37	1.48
IETest	0.80	0.28	0.28	0.29	0.69	0.54	0.52	0.61	0.77	0.73	1.57
IDTest	11.06	7.94	2.25	2.35	3.84	5.41	7.06	5.88	7.03	12.76	8.56
TCETest	4.80	3.59	3.56	2.45	3.61	3.28	3.17	3.53	3.55	5.26	3.95
TCDTest	7.92	4.82	5.01	4.30	5.79	5.87	7.23	8.14	9.19	12.97	8.62
BHTest	7.85	3.95	2.36	1.80	2.46	4.11	2.97	1.90	3.18	6.14	4.93

Figure 4: RMSDs in kcal/mol for 8 datatypes for 11 density functionals. These datatype RMSDs include data points from the primary and secondary test sets only. NCED stands for non-covalent dimers (easy), NCEC stands for non-covalent clusters (easy), NCD stands for non-covalent dimers (difficult), IE stands for isomerization energies (easy), ID stands for isomerization energies (difficult), TCE stands for thermochemistry (easy), TCD stands for thermochemistry (difficult), and BH stands for barrier heights. The partitioning of the 3548 data points contained in this figure into the 8 datatypes is: 1433, 223, 71, 679, 88, 660, 258, and 136.

Dataset	Datatype	B97-D3(BJ)	B97M-V	ωB97X-V	ωB97M-V	ωB97X-D	ωM05-D	M06-2X	M08-HX	M11	M06-L	MN15-L
A24	NCED	0.28	0.15	0.08	0.09	0.16	0.17	0.26	0.22	0.35	0.35	0.57
DS14	NCED	0.32	0.12	0.11	0.15	0.24	0.24	0.25	0.18	0.55	0.43	0.69
HB15	NCED	0.94	0.28	0.28	0.20	0.51	0.43	0.36	0.45	0.54	0.58	2.32
HSG	NCED	0.55	0.12	0.16	0.11	0.35	0.29	0.52	0.68	0.88	0.63	0.83
NBC10	NCED	0.64	0.31	0.33	0.16	0.25	0.38	0.56	0.69	0.87	0.61	1.25
S22	NCED	0.49	0.31	0.27	0.28	0.24	0.36	0.54	0.64	0.88	0.83	2.52
X40	NCED	0.52	0.19	0.24	0.22	0.55	0.53	0.32	0.50	0.74	0.59	1.18
H2O6Bind8	NCEC	3.32	0.34	0.43	0.29	0.83	0.75	1.60	0.65	0.97	1.35	10.01
HW6Cl	NCEC	1.90	0.21	0.34	0.22	0.39	0.94	2.84	2.31	0.93	0.90	5.18
HW6F	NCEC	5.04	0.59	0.13	0.14	0.67	2.00	4.07	2.02	1.69	1.23	5.83
TA13	NCD	5.31	4.12	2.88	2.75	2.91	2.57	1.38	1.65	1.82	3.78	1.77
XB18	NCD	0.38	0.57	0.51	0.42	0.98	1.06	0.58	0.79	1.21	0.39	0.75
AlkIsomer11	IE	1.14	0.25	0.69	0.19	1.06	0.33	0.18	0.34	0.54	0.88	1.84
Butanediol65	IE	0.35	0.19	0.04	0.04	0.20	0.18	0.19	0.33	0.37	0.23	1.18
EIE22	ID	1.98	2.29	0.26	0.24	0.69	0.53	0.37	0.51	0.54	2.65	2.07
Styrene45	ID	6.87	4.34	3.95	1.92	2.07	2.50	2.98	2.38	3.62	5.79	4.55
AlkAtom19	TCE	2.04	1.04	1.69	0.91	3.35	6.46	8.02	7.38	5.42	9.63	17.04
BDE99nonMR	TCE	4.07	3.56	3.14	2.50	2.68	2.71	2.77	3.52	3.76	5.66	3.81
G21EA	TCE	3.35	2.57	3.08	2.82	2.45	2.75	2.81	2.77	2.10	5.15	2.90
G21IP	TCE	4.51	3.64	3.56	3.69	3.82	3.57	3.57	4.59	4.85	5.45	4.25
TAE140nonMR	TCE	4.85	3.89	2.95	2.23	3.01	2.77	2.98	2.88	3.74	5.43	4.30
BHPERI26	BH	4.24	1.43	2.75	1.44	2.40	1.82	1.81	1.97	2.71	2.18	2.12
CRBH20	BH	14.16	7.56	3.16	1.23	1.66	0.80	1.58	1.31	1.25	13.73	7.18
DBH24	BH	7.63	4.95	1.75	1.46	2.03	1.91	1.08	1.30	1.42	5.24	3.22

Figure 5: RMSDs in kcal/mol for 24 of the 25 training datasets (AE18 is excluded) for 11 density functionals. Table 1 contains information regarding the datasets, and the datatypes are explained in Section 3.

Moving away from the relatively unimportant training datasets toward the more meaningful primary test datasets (Figure 6), the performance of ωB97M-V is generally satisfactory, and the new functional has the smallest RMSD for 15 of the 34 primary test datasets considered. In order to circumvent the laborious process of documenting the performance of ωB97M-V for all 34 primary test datasets in Figure 6, only a handful of the datasets will be analyzed.

The S66 dataset[68,69] is certainly the most popular of the NCED datasets in the primary test set, and the performance of ωB97M-V is very good. Its RMSD of 0.15 kcal/mol is slightly larger than that of ωB97X-V (0.13 kcal/mol), which is the best performer. ωB97M-V performs more than 2 times better than M06-2X, nearly 3 times better than ωB97X-D, and about 4 times better than M11. At 0.18 kcal/mol, B97M-V has the third smallest RMSD, and is the best local functional tested.

The Shields38 dataset[79] contains 38 water clusters, ranging from dimers to decamers. ωB97M-V performs the best, with an RMSD of 0.48 kcal/mol, followed by M08-HX, with an RMSD of 0.51 kcal/mol, and B97M-V, ωB97X-V, and ωB97X-D, which have RMSDs around 0.7 kcal/mol. The rest of the functionals have RMSDs between 1 and 3 kcal/mol, with the exception of MN15-L, which performs very poorly (10.44 kcal/mol). Binding energies for larger clusters are evaluated later on, with the 14 water 20-mers in the secondary test set.

The CYCONF dataset is taken from the GMTKN30 database[82,95] and contains the isomerization energies of 10 cysteine conformers. Again, ωB97M-V performs the best for this dataset, with a small RMSD of 0.07 kcal/mol that is virtually indistinguishable from that of ωB97X-V, and nearly 3.5 times better than that of the next best functional, M06-2X.

The HAT707nonMR dataset from the W4-11 database[103] contains 505 heavy-atom transfer energies, and is one of the largest datasets in the primary test set. ωB97M-V affords an impressive RMSD of 2.64 kcal/mol on this dataset, performing nearly 25% better than the next best functional, M06-2X (3.27 kcal/mol), and 45% better than ωB97X-V (3.84 kcal/mol).

The most interesting datasets contained in this paper are found in the secondary test set, as most of them are taken from papers that were very recently published. Furthermore, the secondary test set is the truest form of transferability testing, as it was compiled and evaluated after ωB97M-V was fully self-consistently trained. Thus, the bulk of the remaining discussion in this section will be focused on the datasets from the secondary test set (Figure 7).

3B-69-DIM is a dataset created from the 3B-69 dataset of Beran and coworkers,[70] and contains all relevant pairs of monomers that can be constructed from the 69 trimers. This results in a total of 207 dimer binding energies and serves as a stringent test of transferability for the new functional. ωB97M-V performs outstandingly for this dataset, with an RMSD of 0.16 kcal/mol, followed by ωB97X-V and B97M-V, with RMSDs of 0.20 and 0.21 kcal/mol, respectively. The next best functional, ωM05-D, performs nearly 2 times worse than ωB97M-V, while the best Minnesota functional, M06-2X, performs more than 3 times worse.

The HB49 dataset[73–75] is a very interesting dataset constructed by Boese, and contains the binding energies of 49 hydrogen-bonded dimers. In fact, a recent benchmark of density functionals on the HB49 dataset found that MP2 at the basis set limit, with an RMSD of approximately 0.3 kcal/mol, performed better than all of the tested Rung 1-4 density functionals. Therefore, it is of interest to assess the performance of ωB97M-V on the HB49 dataset. The results are very encouraging: with a low RMSD of 0.23 kcal/mol, ωB97M-V is the only functional tested which significantly outperforms MP2. In addition, ωB97X-V performs very comparably to MP2, with an RMSD of 0.29 kcal/mol. From the local functionals, B97M-V performs best, with an RMSD of 0.47 kcal/mol.

While the 3B-69 dataset was originally intended as a benchmark for three-body intermolecular interaction energies, it can also be used as a benchmark for trimer binding energies (3B-69-TRIM). This is a good transferability test for ωB97M-V, since very few trimers

Dataset	Datatype	B97-D3(BJ)	B97M-V	ωB97X-V	ωB97M-V	ωB97X-D	ωM05-D	M06-2X	M08-HX	M11	M06-L	MN15-L
A21x12	NCED	0.18	0.09	0.05	0.05	0.10	0.10	0.14	0.18	0.18	0.22	0.40
BzDC215	NCED	0.35	0.22	0.21	0.19	0.31	0.28	0.34	0.49	0.31	0.34	0.77
HW30	NCED	0.37	0.13	0.14	0.17	0.31	0.31	0.37	0.34	0.36	0.51	0.56
NC15	NCED	0.18	0.07	0.06	0.05	0.18	0.16	0.14	0.15	0.22	0.26	0.09
S66	NCED	0.42	0.18	0.13	0.15	0.41	0.53	0.33	0.38	0.61	0.61	2.16
S66x8	NCED	0.35	0.19	0.21	0.11	0.34	0.39	0.38	0.58	0.57	0.52	1.60
FmH2O10	NCEC	10.34	0.17	0.18	0.43	2.88	4.67	8.53	3.01	1.73	3.33	17.61
Shields38	NCEC	2.75	0.69	0.70	0.48	0.73	1.75	1.77	0.51	1.19	1.47	10.44
SW49Bind345	NCEC	0.82	0.38	0.31	0.27	0.76	0.70	0.57	0.60	0.88	0.42	2.15
SW49Bind6	NCEC	1.57	0.81	0.64	0.60	0.70	0.70	0.90	1.15	1.88	0.44	5.11
WATER27	NCEC	2.66	1.37	0.92	0.51	0.65	2.61	2.73	1.26	1.14	1.43	8.49
Bauza30	NCD	2.31	2.07	0.81	0.60	1.34	0.88	1.30	1.14	1.10	1.95	2.07
CT20	NCD	0.43	0.29	0.11	0.11	0.50	0.34	0.23	0.35	0.52	0.40	0.33
XB51	NCD	1.77	0.94	1.48	1.29	1.13	1.01	0.73	0.98	1.97	0.89	1.08
ACONF	IE	0.10	0.13	0.02	0.07	0.27	0.24	0.29	0.46	0.73	0.49	0.85
CYCONF	IE	0.70	0.27	0.09	0.07	0.40	0.29	0.24	0.33	0.40	0.40	0.56
Pentane14	IE	0.28	0.31	0.08	0.13	0.16	0.20	0.13	0.29	0.49	0.38	0.43
SW49Rel345	IE	0.76	0.10	0.23	0.13	0.86	0.68	0.24	0.32	0.31	0.43	0.66
SW49Rel6	IE	1.08	0.10	0.27	0.18	1.20	0.87	0.33	0.26	0.24	0.73	0.98
DIE60	ID	1.75	1.93	0.82	0.65	0.79	0.96	0.84	0.96	0.97	2.63	2.08
ISOMERIZATION20	ID	3.81	2.85	1.59	1.91	1.80	1.23	1.50	1.78	2.24	3.87	2.93
AlkIsod14	TCE	2.24	0.58	1.84	1.05	2.37	1.48	1.72	1.93	2.14	3.93	0.83
BH76RC	TCE	4.07	2.71	1.89	1.22	1.79	1.37	1.20	1.55	2.10	4.18	3.26
EA13	TCE	3.73	2.48	2.96	2.21	2.30	2.96	2.51	1.53	0.75	5.10	3.09
HAT707nonMR	TCE	5.07	3.88	3.84	2.64	3.69	3.52	3.27	3.80	3.80	5.36	4.17
IP13	TCE	3.49	3.81	3.36	3.12	3.17	2.93	3.18	4.10	5.45	2.71	2.36
NBPRC	TCE	3.66	1.93	2.06	1.06	2.15	1.07	1.28	2.13	3.37	4.72	3.08
SN13	TCE	3.50	1.37	0.98	0.58	0.98	1.02	0.91	0.90	1.83	1.58	2.64
BDE99MR	TCD	6.60	3.04	4.86	4.33	5.22	6.52	7.33	7.62	6.72	4.27	2.42
HAT707MR	TCD	7.11	3.33	4.82	4.18	4.39	5.08	6.25	6.57	6.44	5.25	3.48
TAE140MR	TCD	12.29	5.70	5.45	5.28	6.02	6.17	8.49	9.15	7.73	6.30	4.48
CR20	BH	9.53	2.15	2.90	0.56	3.68	1.64	2.07	2.56	6.24	12.70	1.68
HTBH38	BH	8.28	4.60	2.36	1.72	2.69	2.81	1.29	1.25	1.73	4.66	1.81
NHTBH38	BH	7.58	5.30	1.69	1.98	1.86	1.70	1.67	1.57	1.49	4.86	3.46

Figure 6: RMSDs in kcal/mol for 34 of the 35 primary test datasets (RG10 is excluded) for 11 density functionals. Table 1 contains information regarding the datasets, and the datatypes are explained in Section 3.

are found in its training set. ωB97M-V performs very well for this dataset, with the smallest RMSD of 0.32 kcal/mol. The next best functionals are ωB97X-V and B97M-V, with RMSDs of 0.39 and 0.47 kcal/mol, respectively. Only two other functionals manage RMSDs under 1 kcal/mol: ωM05-D and ωB97X-D, with RMSDs of 0.65 and 0.88 kcal/mol, respectively.

Having tested the performance of ωB97M-V for small- to medium-sized water clusters with the Shields38 dataset in the primary test set, it is time to consider the H2O20Bind10 and H2O20Bind4 datasets in the secondary test set, as they contain a total of 14 water 20-mer binding energies. In order to address both datasets simultaneously, the geometric mean of the two RMSDs (GMRMSD) will be considered. ωB97M-V performs best overall, with a GMRMSD of 1.01 kcal/mol, while ωB97X-D and ωB97X-V perform second and third best, with GMRMSDs of 1.38 and 1.48 kcal/mol. ωM05-D and B97M-V perform very similarly, with GMRMSDs around 2.85 kcal/mol, while M06-2X is the best of the tested Minnesota functionals, with a GMRMSD of 3.40 kcal/mol.

While the binding energies of small, medium, and large water clusters have been thoroughly addressed thus far, it is important to assess the performance of ωB97M-V for the relative energies of water clusters. This is done with the help of three datasets from the secondary test set: H2O16Rel5, H2O20Rel10, and H2O20Rel4. Once again, the geometric mean of these three datasets will be considered for brevity. The GMRMSD of ωB97M-V across these three datasets is remarkably small, at only 0.09 kcal/mol. The next best functionals are ωB97X-D and ωB97X-V, with very similar GMRMSDs of 0.22 and 0.24 kcal/mol, respectively. B97M-V is the best local functional, with a GMRMSD of 0.41 kcal/mol, while the two remaining non-Minnesota functionals (ωM05-D and B97-D3(BJ)) have GMRMSDs of 0.67 and 1.04 kcal/mol, respectively. None of the Minnesota functionals are able to obtain a GMRMSD under 1 kcal/mol for these isomerization energies.

A recent benchmark by Karton and coworkers on the YMPJ519 dataset of amino acid isomerization energies[99] found ωB97X-V to be the best Rung 1-4 density functional. Thus, it is important to verify that ωB97M-V performs as well as its GGA counterpart. Accordingly, both ωB97X-V and ωB97M-V have impressive RMSDs of 0.30 and 0.32 kcal/mol, respectively, while the smallest RMSD is surprisingly reserved for B97M-V, at 0.28 kcal/mol. The rest of the functionals have RMSDs that range from 0.49 kcal/mol (M06-2X) to 1.51 kcal/mol (MN15-L).

Another recent benchmark by Martin and coworkers assessed the performance of various density functionals for the relative energies of a handful of C_{20} and C_{24} structures.[104] The study found that only double hybrid functionals were able to afford RMSDs under 10 kcal/mol (with the smallest RMSD being around 8.3 kcal/mol). Therefore, it is interesting to assess the performance of ωB97M-V on this dataset to see if it can break the 10 kcal/mol barrier. Both ωB97X-V and ωB97M-V manage RMSDs under 7 kcal/mol, with the former slightly outperforming the latter. By contrast, the best local functional is B97M-V with an RMSD of 25.39 kcal/mol, followed closely by MN15-L (27.43 kcal/mol). From the remaining hybrid functionals, ωB97X-D, ωM05-D, and M08-HX manage RMSDs under 20 kcal/mol, while M11 and M06-2X perform more than 3 times worse than ωB97M-V.

A very challenging benchmark set by Martin and coworkers[114] assessed the performance of density functionals for various reactions (homodesmotic, isodesmic, and isogyric) involving platonic hydrocarbon cages, in addition to their atomization energies. While the individual RMSDs for these four datasets are given in Figure 7, the functionals will be assessed based on the geometric mean of the four RMSDs. Although the original study found ωB97X-V to be the most promising Rung 1-4 functional overall, ωB97M-V manages a GMRMSD of only 3.86 kcal/mol, compared to ωB97X-V's GMRMSD of 5.99 kcal/mol. Thus, ωB97M-V improves over ωB97X-V by over 50%. The next best functional (B97M-V) is surprisingly a local one, and has a GMRMSD of 7.27 kcal/mol. The performance of B97M-V is certainly note-

worthy, since the two local Minnesota functionals have GMRMSDs larger than 20 kcal/mol. While M06-2X and M08-HX perform 3 times worse than ωB97M-V, M11 performs more than 4.5 times worse than ωB97M-V.

6.3 Potential Energy Curves

Within the NCED category, the BzDC215, NBC10, and S66x8 datasets contain potential energies curves (PEC) that can be used to assess the accuracy of density functionals for predicting equilibrium properties of dimers. Furthermore, the RG10 dataset contains all 10 PECs that can be constructed between the rare-gas dimers from helium to krypton. In total, these four datasets contain 96 PECs, with BzDC215, NBC10, and RG10 each having 10, and S66x8 having 66. Unfortunately, even with the (99,590)/SG-1 grid, some of the resulting potential energy curves are too oscillatory to be accurately interpolated,[127–129] primarily for the Minnesota density functionals. Consequently, the benzene-neon dimer and the benzene-argon dimer PECs from BzDC215 were removed, the sandwich benzene dimer, the methane dimer, and the sandwich (S2) pyridine dimer PECs from NBC10 were removed, and the helium dimer PEC from RG10 was removed, leaving a total of 90 potential energy curves. Figure 8 contains the equilibrium bond length (EBL) and equilibrium binding energy (EBE) RMSDs for these four datasets, along with the corresponding total RMSDs with RG10 excluded (All*). In order to keep the discussion succinct, only the RG10 and All* results will be discussed.

For the nine rare-gas dimers, the three VV10-containing functionals predict reasonably accurate equilibrium bond lengths, with RMSDs around 0.07 Å. The only other functional that manages an EBL RMSD of under 0.1 Å for the rare-gas dimers is MN15-L. However, it is important to mention that MN15-L was fit to at least a single point from the PEC of six of the nine rare-gas dimers considered here. The rest of the Minnesota functionals perform very poorly, with RMSDs between 0.2 and 0.7 Å. ωB97X-D also performs poorly, with an RMSD of 0.403, while the worst overall performer is ωM05-D, with an RMSD of 0.722 Å.

Moving on to the 81 PECs in the All* category, the best performance is exhibited by ωB97M-V, with a very impressive equilibrium bond length RMSD of only 0.014 Å. In fact, ωB97M-V performs almost 2 times better than the next best functional, B97M-V, and 3 times better than ωB97X-V. The five Minnesota functionals have RMSDs that range from 0.043 Å (M06-L) to 0.088 Å (M08-HX and MN15-L), while ωM05-D, a range-separated hybrid functional based on the M05 functional form,[30] performs almost as well as B97M-V, with an RMSD of 0.027 Å.

As for the All* equilibrium binding energies, ωB97M-V, ωB97X-V, and B97M-V perform very well, with RMSDs between 0.15 and 0.17 kcal/mol, while the rest of the functionals (except MN15-L) have RMSDs that lie between 0.3 and 0.6 kcal/mol. MN15-L, on the other hand, has an All* EBE RMSD of nearly 2 kcal/mol, which is more than 3 times larger than that of M06-L.

Although the benzene-argon dimer was removed from the BzDC215 dataset in order to generate the RMSDs discussed thus far, it is nevertheless an interesting example of a system bound primarily by dispersion. Furthermore, due to the inherent weakness of the interaction, it is a case that can be used to assess the sensitivity of density functionals (especially meta-GGAs) to the integration grid. Figure 9 displays the PEC for the benzene-argon dimer as calculated by 6 of the 11 benchmarked density functionals with the (99,590)/SG-1 grid. It is evident that the grid filtering that was applied in Section 5 worked successfully, since the PEC of ωB97M-V is nearly as smooth as that of ωB97X-V for this system. By contrast, the Minnesota functionals are far harder to converge with respect to the grid, with M06-2X appearing to behave better than either M06-L or MN15-L.

Considering the accuracy of the PECs themselves, ωB97M-V, ωB97X-V, and B97M-V are very accurate, with equilibrium bond length errors of -0.008, -0.01, and -0.026 Å, respectively. M06-2X has an EBL error that is around 0.1 Å

Dataset	Datatype	B97-D3(BJ)	B97M-V	ωB97X-V	ωB97M-V	ωB97X-D	ωM05-D	M06-2X	M08-HX	M11	M06-L	MN15-L
3B-69-DIM	NCED	0.48	0.21	0.20	0.16	0.39	0.29	0.52	0.74	0.87	0.72	1.27
AlkBind12	NCED	0.38	0.20	0.12	0.13	1.00	1.18	0.30	0.28	0.51	0.38	3.49
CO2Nitrogen16	NCED	0.58	0.21	0.10	0.09	0.81	0.62	0.36	0.58	0.86	1.16	0.82
HB49	NCED	0.76	0.47	0.29	0.23	0.37	0.56	0.56	0.48	0.63	0.72	2.00
Ionic43	NCED	1.33	0.67	0.78	0.70	1.07	0.83	1.16	1.38	1.63	1.02	2.39
3B-69-TRIM	NCEC	1.11	0.47	0.39	0.32	0.88	0.65	1.31	1.90	2.14	1.71	2.70
CE20	NCEC	1.78	0.82	0.69	0.65	0.42	1.42	1.44	0.45	1.70	1.34	6.32
H2O20Bind10	NCEC	17.87	2.76	1.18	0.97	1.95	1.36	3.50	3.91	9.86	6.32	46.44
H2O20Bind4	NCEC	10.62	2.96	1.87	1.06	0.98	5.91	3.30	4.75	9.44	8.10	40.25
H2O16Rel5	IE	1.40	0.41	0.38	0.04	0.11	0.56	1.91	1.08	1.43	2.21	5.03
H2O20Rel10	IE	0.45	0.32	0.11	0.12	0.40	0.67	1.44	0.94	1.07	1.33	2.43
H2O20Rel4	IE	1.78	0.53	0.30	0.14	0.23	0.79	1.92	0.93	1.24	3.01	5.92
Melatonin52	IE	0.52	0.37	0.11	0.16	0.31	0.35	0.27	0.47	0.74	0.88	1.55
YMPJ519	IE	0.82	0.28	0.30	0.32	0.71	0.54	0.49	0.64	0.80	0.65	1.51
C20C24	ID	35.87	25.39	6.66	6.97	12.23	17.65	23.20	19.12	22.90	41.27	27.43
BSR36	TCE	4.01	0.35	2.87	1.11	5.19	2.62	4.46	3.50	2.46	7.00	3.63
HNBrBDE18	TCE	4.72	4.21	2.55	2.62	4.29	3.65	3.07	0.95	1.79	5.21	4.19
WCPT6	TCE	1.19	0.99	1.07	0.36	1.10	0.72	0.87	0.83	1.64	2.28	0.99
PlatonicHD6	TCD	10.73	5.27	4.89	4.33	4.43	4.88	9.12	6.07	12.91	25.53	15.80
PlatonicID6	TCD	6.99	5.05	5.01	1.92	10.06	9.74	14.37	11.42	10.14	16.65	18.37
PlatonicIG6	TCD	6.08	20.93	6.95	6.55	22.00	10.72	11.21	22.84	33.02	70.12	42.97
PlatonicTAE6	TCD	16.62	5.01	7.55	4.07	4.55	12.73	13.65	18.19	24.46	17.38	16.90
PX13	BH	6.46	1.60	3.38	2.55	1.62	9.62	6.94	3.02	4.45	1.66	12.85
WCPT27	BH	6.72	2.15	2.12	1.82	2.05	4.82	3.42	1.79	2.25	2.24	4.38

Figure 7: RMSDs in kcal/mol for the 24 secondary test datasets for 11 density functionals. Table 1 contains information regarding the datasets, and the datatypes are explained in Section 3.

Dataset	B97-D3(BJ)	B97M-V	ωB97X-V	ωB97M-V	ωB97X-D	ωM05-D	M06-2X	M08-HX	M11	M06-L	MN15-L
BzDC215	0.036	0.036	0.039	0.034	0.043	0.034	0.101	0.119	0.095	0.064	0.049
NBC10	0.037	0.040	0.050	0.024	0.044	0.042	0.091	0.114	0.076	0.099	0.134
RG10	0.220	0.065	0.062	0.075	0.403	0.722	0.247	0.353	0.673	0.311	0.095
S66x8	0.047	0.022	0.041	0.007	0.037	0.024	0.071	0.081	0.067	0.027	0.085
All* EBL	0.045	0.026	0.042	0.014	0.038	0.027	0.077	0.088	0.071	0.043	0.088
BzDC215	0.47	0.11	0.23	0.24	0.39	0.39	0.44	0.54	0.35	0.44	1.14
NBC10	0.67	0.20	0.17	0.15	0.27	0.45	0.46	0.48	0.82	0.75	1.62
RG10	0.05	0.04	0.03	0.05	0.08	0.16	0.11	0.14	0.17	0.14	0.02
S66x8	0.38	0.17	0.13	0.13	0.44	0.52	0.30	0.34	0.57	0.60	2.05
All* EBE	0.42	0.17	0.15	0.15	0.42	0.50	0.33	0.38	0.58	0.60	1.94

Figure 8: Equilibrium bond length (EBL) RMSDs in Å and equilibrium binding energy (EBE) RMSDs in kcal/mol for 11 density functionals. The first section contains the EBL RMSDs while the second section contains the EBE RMSDs. The All* category contains 81 data points and is a combination of BzDC215, NBC10, and S66x8. More information regarding the datasets and excluded potential energy curves can be found in Table 1 and Section 6.3, respectively.

in magnitude, while M06-L overestimates the bond length by at least 0.3 Å. The three VV10-containing functionals manage to reproduce the equilibrium binding energy rather well, with the largest error (12%) attributed to ωB97X-V, a 7.5% error attributed to ωB97M-V, and the smallest error associated with B97M-V (2%). Despite predicting a bond length that is more than 0.1 Å too short, M06-2X underestimates the EBE of the benzene-argon dimer by only 6.5%. By contrast, MN15-L overbinds the system by more than 1.15 kcal/mol.

7 Reaching the Basis Set Limit

Although ωB97M-V was consistently trained and tested in the def2-QZVPPD basis set (without counterpoise corrections), it is inevitable that it will be used with different basis sets. As a result, this section explores the use of ωB97M-V with 21 basis sets from 4 different families, and makes recommendations based on how closely these basis sets can mimic the results of the training set basis (TSB), def2-QZVPPD. For this purpose, four datasets are selected and tested: S66 representing non-covalent interactions, Pentane14 representing isomerization energies, AlkAtom19 representing thermochemistry, and CRBH20 representing barrier heights. For the S66 dataset, the calculations are performed both with and without counterpoise corrections (designated CP and noCP, respectively), because it is very unlikely that a double- or triple-zeta basis set without counterpoise corrections will be able to reproduce the quadruple-zeta, def2-QZVPPD basis set binding energies. The results, summarized in Figure 10, are analyzed using two sets of RMSDs (the first relative to the reference values and the second relative to the def2-QZVPPD values) for each of the five datasets of interest: S66 CP, S66 noCP, Pentane14, AlkAtom19, and CRBH20. In order to facilitate the use of Figure 10, the basis sets are sorted based on the geometric mean (GM) of the S66 CP, Pentane14, AlkAtom19, and CRBH20 RMSDs relative to the TSB. The S66 noCP RMSD is excluded from the GM because it unfairly disadvantages triple-zeta basis sets. Furthermore, the RMSDs within each dataset are color-coded, with green indicating that the use of the corresponding basis set with the type of interaction represented by the corresponding dataset is recommended, yellow indicating that the pairing should be used with caution, and red indicating that the pairing should not be used. Finally, the number of basis functions that each basis set contains for octane is shown in the last column of Figure 10.

From the outset, it is clear that a handful of basis sets are entirely incompatible with ωB97M-V, namely def2-SVP, def2-SVPD, pc-0, aug-pc-0, pc-1, aug-pc-1, and cc-pVDZ. This result is expected, since the functional is trained as close to the basis set limit as possible. On the other hand, it is clear that certain basis sets are very compatible with ωB97M-V, namely pc-3, aug-pc-3, aug-cc-pVQZ, and of course, def2-QZVPPD. These basis sets work superbly well for isomerization energies, thermochemistry, and barrier heights, and provide accurate binding energies for non-covalent interactions with and even without counterpoise corrections. With counterpoise corrections, aug-pc-2 and def2-QZVPP additionally provide satisfactory results for all four types of interactions. While the smallest basis set that can successfully handle all four categories is aug-pc-2 with 274 basis functions for octane, two smaller basis sets, pc-2 and def2-TZVPPD, are almost always satisfactory, with the former being considerably smaller than aug-pc-2. In fact, the only result that makes pc-2 not fully satisfactory is the S66 CP RMSD relative to the TSB (0.11 kcal/mol). However, the RMSD relative to the reference values is actually very impressive (0.13 kcal/mol). Thus, pc-2, with only 188 basis functions for octane, is the most economical option that can be recommended for use with ωB97M-V. def2-TZVPPD, on the other hand, has an RMSD of 2.75 kcal/mol for AlkAtom19, relative to the TSB. However, the RMSD of 1.86 kcal/mol relative to the reference values is still acceptable, making def2-TZVPPD, with only 230 basis functions for octane, another economical basis set choice. The

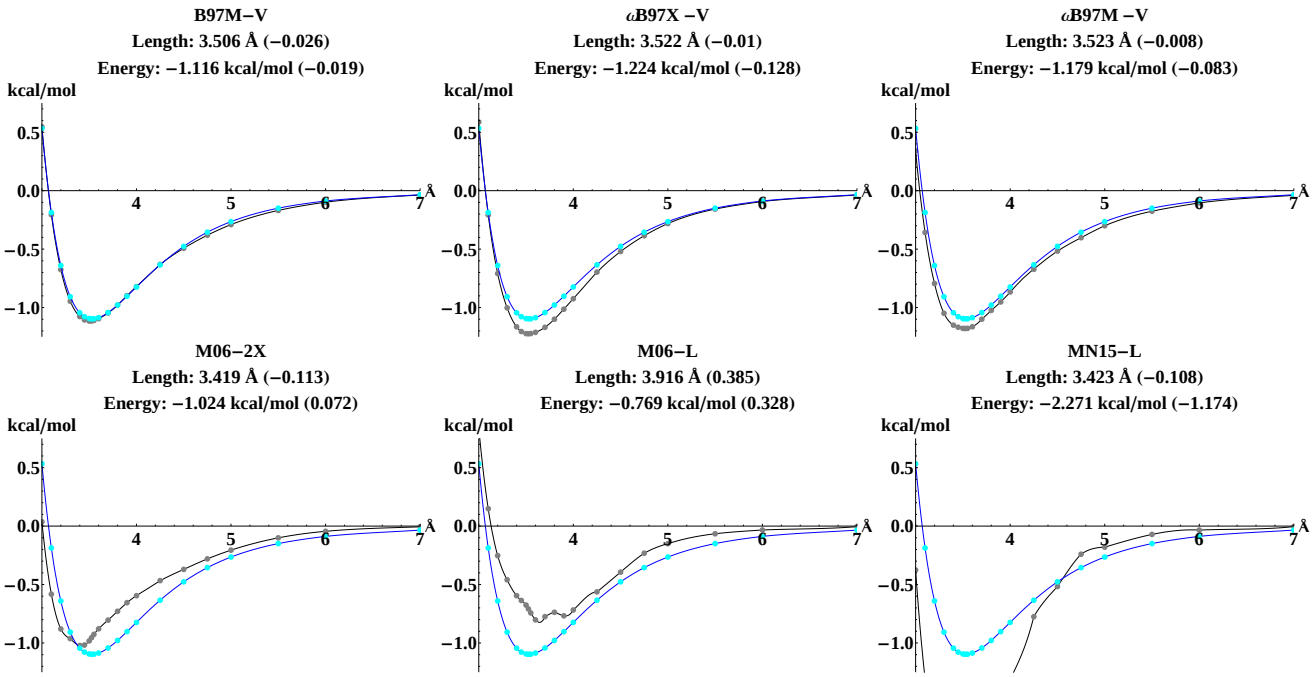

Figure 9: Potential energy curves for the benzene-argon dimer from BzDC215 as computed by 6 of the 11 benchmarked density functionals. The gray curve represents the DFT method, while the blue curve represents the reference method. The line immediately following the functional name contains the equilibrium bond length in Å and the error (with respect to the reference) in parentheses. The following line contains the same information for the equilibrium binding energy (in kcal/mol).

rest of the basis sets that have not been mentioned explicitly must be used very cautiously.

8 Reaching the Integration Grid Limit

Different density functionals converge to the integration grid limit at different rates. During the training process of ωB97M-V, the billions of candidate functionals were filtered such that the least-squares fit energies generated in the (99,590)/SG-1 and (250,974)/SG-1 grids differed by an absolute maximum of 0.015 kcal/mol. The effectiveness of this decision is tested by analyzing the grid sensitivity of ωB97M-V on all of the datasets in the training and primary test sets (with the exception of AE18 and RG10) with the following grids: (250,974)/SG-1, (99,590)/SG-1, (99,302)/SG-1, (75,590)/SG-1, (75,302)/SG-1, (75,302)/SG-0, and SG-1/SG-0.

Table 5 summarizes the results of this comprehensive test involving 3248 data points, which are binned with respect to the absolute error (AE) in kcal/mol. The table is populated with the assumption that the (250,974)/SG-1 results are fully converged with respect to the grid. Starting with the (99,590)/SG-1 grid, it is clear that the filtering applied during the training stage has completely transferred to the final functional form, since all 3248 data points have absolute errors less than 0.015 kcal/mol. Furthermore, changing the number of radial shells from 99 to 75 (while keeping the number of angular grid points constant) seems to have a negligible effect on the results, yet accelerates the integration of the local exchange-correlation functional by 25%. On the other hand, changing the number of angular grid points from 590 to 302 (while keeping the number of radial shells constant) seems to have a much more profound effect. Based on the negligible effect of transitioning from (99,590)/SG-1 to (75,590)/SG-1, it is reasonable to assume that transitioning from (99,302)/SG-1 to (75,302)/SG-1 should

Dataset	S66 noCP		S66 CP		Pentane14		AlkAtom19		CRBH20		GM	BF
Comparison	vs. Ref	vs. TSB	vs. Ref	vs. TSB	vs. Ref	vs. TSB	vs. Ref	vs. TSB	vs. Ref	vs. TSB	vs. TSB	C_8H_{18}
def2-QZVPPD	0.15	0.00	0.14	0.00	0.13	0.00	0.91	0.00	1.23	0.00	0.00	350
def2-QZVPP	0.18	0.13	0.14	0.02	0.13	0.00	0.85	0.05	1.20	0.03	0.02	316
aug-cc-pVQZ	0.15	0.03	0.14	0.01	0.13	0.00	0.66	0.25	1.20	0.11	0.03	412
aug-pc-3	0.15	0.02	0.14	0.01	0.12	0.01	0.21	0.76	1.14	0.12	0.05	472
pc-3	0.14	0.03	0.14	0.01	0.12	0.01	0.22	0.74	1.13	0.14	0.05	360
aug-pc-2	0.18	0.08	0.13	0.04	0.12	0.02	0.82	0.09	1.29	0.14	0.06	274
def2-TZVPPD	0.19	0.10	0.13	0.02	0.12	0.01	1.86	2.75	1.20	0.06	0.08	230
pc-2	0.26	0.27	0.13	0.11	0.14	0.02	1.11	0.21	1.18	0.19	0.09	188
cc-pVQZ	0.41	0.41	0.16	0.07	0.13	0.00	1.06	1.95	1.24	0.17	0.10	300
aug-cc-pVTZ	0.27	0.19	0.15	0.04	0.17	0.04	2.62	1.72	1.27	0.27	0.16	274
def2-TZVPP	0.43	0.42	0.15	0.08	0.15	0.03	1.68	2.58	1.13	0.13	0.17	196
LP	0.58	0.51	0.19	0.12	0.16	0.06	0.24	0.98	1.26	0.16	0.18	216
cc-pVTZ	0.96	0.97	0.21	0.15	0.15	0.03	0.80	1.69	1.28	0.45	0.25	188
aug-pc-1	1.93	1.87	0.24	0.18	0.21	0.11	13.80	12.90	1.66	0.81	0.68	162
aug-cc-pVDZ	0.90	0.85	0.20	0.13	0.36	0.25	14.85	13.95	0.71	1.17	0.85	162
cc-pVDZ	2.34	2.35	0.49	0.47	0.09	0.18	6.00	5.09	1.28	1.32	0.86	102
pc-1	2.05	2.05	0.58	0.58	0.10	0.14	13.88	12.99	4.37	3.41	1.39	102
def2-SVP	2.46	2.47	0.41	0.42	0.21	0.24	27.50	28.40	2.10	3.04	1.71	102
def2-SVPD	1.69	1.65	0.27	0.23	0.54	0.43	34.47	35.37	1.79	2.68	1.75	136
aug-pc-0	4.98	4.96	1.51	1.58	0.68	0.59	31.27	30.38	5.37	6.06	3.62	110
pc-0	7.16	7.18	1.51	1.57	0.77	0.68	40.43	41.32	11.04	11.96	4.79	76

Figure 10: RMSDs in kcal/mol for 4 datasets computed with 21 different basis sets. S66 represents non-covalent interactions, Pentane14 represents isomerization energies, AlkAtom19 represents thermochemistry, and CRBH20 represents barrier heights. The S66 dataset is computed both with and without counterpoise corrections (designated CP and noCP, respectively). The RMSDs are taken with respect to both the reference values (vs. Ref) as well as the training set basis (vs. TSB). The basis sets are sorted based on the geometric mean (GM) of the S66 CP, Pentane14, AlkAtom19, and CRBH20 RMSDs relative to the TSB. The S66 noCP RMSD is excluded from the GM because it unfairly disadvantages triple-zeta basis sets. The number of basis functions (BF) that each basis set contains for octane is shown in the last column.

have a negligible effect on the (99,302)/SG-1 results. The (75,302)/SG-1 results indicate that this is indeed true.

The goal of this grid analysis is to recommend three tiers of integration grids for use with ωB97M-V: fine, medium, and coarse. So far, it is clear that the (99,590)/SG-1 grid is certainly the finest grid that is necessary to obtain fully converged results. Thus, the (99,590)/SG-1 grid is deemed to be the "fine" option for ωB97M-V. Furthermore, the only other combination that is computationally more efficient than the (99,590)/SG-1 grid yet maintains its accuracy is the (75,590)/SG-1 grid, which receives the "medium" certification. While (75,302)/SG-1 appears to be a viable coarse option, it is useful to see if the nonlocal grid can be reduced without incurring substantial additional errors. Modifying the nonlocal grid from SG-1 to SG-0 (while maintaining the (75,302) local grid) only negligibly affects the results. On the other hand, modifying the local grid from (75,302) to SG-1 (with SG-0 as the nonlocal grid) has a devastating effect on the quality of the results and is absolutely not recommended. Therefore, the "coarse" specification is deemed to be the (75,302)/SG-0 grid.

Based on these results, the following three grids are recommended for use with ωB97M-V:

- fine: (99,590)/SG-1
- medium: (75,590)/SG-1
- coarse: (75,302)/SG-0

9 Conclusions

For semi-empirical density functionals, universality (or transferability) is impossible to fully guarantee, because such functionals are necessarily approximate. In other words, for a given system, a new density functional *cannot necessarily* improve over existing ones, even though it may *often* do so. Nonetheless, within a class of functionals, transferability can be enhanced by minimizing the number of empirical parameters (i.e. avoiding overfitting), while increasing the size of the training and test sets. Even then, the use of a new density functional should only be advocated if it *statistically* improves upon a wide variety of existing competitors in and below its class, across a very diverse set of benchmark systems.

ωB97M-V was developed upon these foundations. A combinatorial, "survival-of-the-most-transferable" approach was utilized to screen over 10 billion candidate least-squares fits based on accuracy, transferability, and desired physical properties, an immense database of nearly 5000 data points was used to train and test the most promising fit, and the final, self-consistently-optimized density functional was assessed against 10 well-respected semi-empirical functionals across all 4987 data points. The results are very encouraging, beginning with a large reduction in the number of trained parameters versus other meta-GGA functionals from 29 (M06-2X), 40 (M11), 47 (M08-HX), or 58 (MN15-L), to 12 in ωB97M-V. *The use of additional parameters did not yield significantly better transferability in the screening and gradually leads to potential problems with overfitting.*

The combined training, primary test, and secondary test set results (summarized in Figure 11) indicate that ωB97M-V is remarkably accurate for non-covalent interactions, isomerization energies, thermochemistry, and barrier heights across the main-group elements. For both NCED and NCEC, ωB97M-V is at least 30% more accurate than the next best tested functional, which is ωB97X-V. ωB97M-V is equivalent to ωB97X-V and B97M-V for IE, but outperforms all tested functionals by at least 30% for ID. Additionally, ωB97M-V is almost 40% more accurate than ωB97X-V for TCE, and 30% more accurate than any tested functional. For TCD, ωB97M-V significantly outperforms the next best functionals, which are B97M-V and ωB97X-V. Finally, despite only having 15% short-range exact exchange, ωB97M-V is the best tested density functional for BH.

ωB97M-V was consistently trained and tested in the def2-QZVPPD basis set (without counterpoise corrections). Thus, it is meant to be used as close as practically possible to the ba-

Table 5: Grid error ranges for 3248 data points from the training and primary test sets. From the original 3835 data points, the 18 data points from AE18 and the 569 data points from RG10 are excluded. The errors are taken with respect to the (250,974)/SG-1 grid. The grids are assessed with respect to the absolute error (AE) in kcal/mol.

AE (kcal/mol)	[0,0.015)	[0.015,0.03)	[0.03,0.045)	[0.045,0.06)	[0.06,0.075)	[0.075,0.09)	[0.09,∞)
(99,590)/SG-1	3248	0	0	0	0	0	0
(75,590)/SG-1	3245	3	0	0	0	0	0
(99,302)/SG-1	3201	39	3	3	2	0	0
(75,302)/SG-1	3190	50	3	3	2	0	0
(75,302)/SG-0	3123	107	11	5	2	0	0
SG-1/SG-0	1851	587	303	160	101	84	162

sis set limit. Its basis set dependence has been thoroughly tested across four types of interactions (non-covalent interactions, isomerization energies, thermochemistry, and barrier heights) in order to identify basis sets that can provide results similar in quality to those acquired with the basis set used for training the parameters. The def2-QZVPPD, pc-3, aug-pc-3, and aug-cc-pVQZ basis sets are recommended for use, both with and without counterpoise corrections (when applicable). Additionally, the def2-QZVPP and aug-pc-2 basis sets are recommended for use with counterpoise corrections (when applicable). Finally, the pc-2 and def2-TZVPPD basis sets (to be used with counterpoise corrections, when applicable) should serve as economical choices under most circumstances.

Since the evaluation of the kinetic energy density is very sensitive to the integration grid, ωB97M-V was trained with the intention of making the (99,590)/SG-1 grid the integration grid limit. This goal was met by filtering fits during the training stage based on their energetic deviation from the (250,974)/SG-1 grid. Based on tests spanning 3248 data points, the (75,302)/SG-0 grid is recommended as a viable coarse option for use with ωB97M-V (particularly for quick calculations), while the (99,590)/SG-1 grid is recommended as the fine option if results near the integration grid limit are required. For most applications, the medium-sized (75,590)/SG-1 grid can serve as a compromise between these two limits.

It is important to discuss the remaining limitations of ωB97M-V. Like most Kohn-Sham density functionals, it is not appropriate for use when strong correlation effects are significant (e.g. see the TCD results in Figure 11). It contains some self-interaction error, which causes larger errors in problems involving odd electrons or holes (e.g. see the NCD results in Figure 11). Additionally, it is trained and tested on main-group elements only, so its performance on transition metal-containing systems remains to be tested as suitable reference values become available. However, the minimal empiricism of ωB97M-V gives reason for cautious optimism in cases such as organometallic systems, where strong correlation is not important.

Finally, it is desirable to apply the same approach used here to develop other semi-empirical density functionals with improved physical content, so that the resulting density functionals are likewise minimally parameterized and optimally transferable. Perhaps the most obvious next step is a range-separated hybrid, meta-GGA density functional that includes nonlocal correlation through virtual orbitals. A functional of this type should have significantly lower errors due to self-interaction. We hope to report such a development in due course.

10 Acknowledgements

This work was supported by the Director, Office of Energy Research, Office of Basic Energy Sciences, Chemical Sciences Division of the U.S. Department of Energy under Contract DE-

Datatype	B97-D3(BJ)	B97M-V	ωB97X-V	ωB97M-V	ωB97X-D	ωM05-D	M06-2X	M08-HX	M11	M06-L	MN15-L
NCED	0.47	0.24	0.24	0.18	0.37	0.38	0.43	0.58	0.65	0.55	1.38
NCEC	4.82	0.95	0.64	0.48	1.01	1.79	2.52	1.73	2.82	2.20	12.83
NCD	2.55	2.01	1.38	1.26	1.49	1.24	0.99	1.05	1.39	1.87	1.47
IE	0.78	0.27	0.27	0.28	0.67	0.52	0.50	0.59	0.74	0.71	1.55
ID	9.15	6.48	2.72	2.05	3.11	4.30	5.56	4.62	5.65	10.16	6.94
TCE	4.66	3.57	3.41	2.48	3.44	3.27	3.29	3.60	3.67	5.44	4.62
TCD	7.92	4.82	5.01	4.30	5.79	5.87	7.23	8.14	9.19	12.97	8.62
BH	8.32	4.35	2.44	1.68	2.34	3.47	2.57	1.80	2.82	6.85	4.78

Figure 11: RMSDs in kcal/mol for 8 datatypes for 11 density functionals. These datatype RMSDs include data points from the training, primary test, and secondary test sets. NCED stands for non-covalent dimers (easy), NCEC stands for non-covalent clusters (easy), NCD stands for non-covalent dimers (difficult), IE stands for isomerization energies (easy), ID stands for isomerization energies (difficult), TCE stands for thermochemistry (easy), TCD stands for thermochemistry (difficult), and BH stands for barrier heights. The partitioning of the 4400 data points contained in this figure into the 8 datatypes is: 1744, 243, 92, 755, 155, 947, 258, and 206.

AC0376SF00098, and by a grant from the SciDac Program.

References

(1) Kohn, W.; Sham, L. J. Self-Consistent Equations Including Exchange and Correlation Effects. *Phys. Rev.* **1965**, *140*, A1133–A1138.

(2) Becke, A. D. Density-functional thermochemistry. V. Systematic optimization of exchange-correlation functionals. *The Journal of Chemical Physics* **1997**, *107*, 8554–8560.

(3) Perdew, J. P.; Ruzsinszky, A.; Tao, J.; Staroverov, V. N.; Scuseria, G. E.; Csonka, G. I. Prescription for the design and selection of density functional approximations: More constraint satisfaction with fewer fits. *The Journal of Chemical Physics* **2005**, *123*, 062201.

(4) Becke, A. D. Density-functional thermochemistry. III. The role of exact exchange. *The Journal of Chemical Physics* **1993**, *98*, 5648–5652.

(5) Gill, P. M. W.; Adamson, R. D.; Pople, J. A. Coulomb-attenuated exchange energy density functionals. *Molecular Physics* **1996**, *88*, 1005–1009.

(6) Grimme, S. Semiempirical GGA-type density functional constructed with a long-range dispersion correction. *Journal of Computational Chemistry* **2006**, *27*, 1787–1799.

(7) Grimme, S.; Antony, J.; Ehrlich, S.; Krieg, H. A consistent and accurate ab initio parametrization of density functional dispersion correction (DFT-D) for the 94 elements H-Pu. *The Journal of Chemical Physics* **2010**, *132*, 154104.

(8) Grimme, S.; Ehrlich, S.; Goerigk, L. Effect of the damping function in dispersion corrected density functional theory. *J. Comput. Chem.* **2011**, *32*, 1456–1465.

(9) Vydrov, O. A.; Voorhis, T. V. Nonlocal van der Waals density functional: The simpler the better. *The Journal of Chemical Physics* **2010**, *133*, 244103.

(10) Lee, K.; Murray, E. D.; Kong, L.; Lundqvist, B. I.; Langreth, D. C. Higher-accuracy van der Waals density functional. *Phys. Rev. B* **2010**, *82*, 081101.

(11) Hamprecht, F. A.; Cohen, A. J.; Tozer, D. J.; Handy, N. C. Development and assessment of new exchange-correlation functionals. *The Journal of Chemical Physics* **1998**, *109*, 6264–6271.

(12) Boese, A. D.; Doltsinis, N. L.; Handy, N. C.; Sprik, M. New generalized gradient approximation functionals. *The Journal of Chemical Physics* **2000**, *112*, 1670–1678.

(13) Boese, A. D.; Handy, N. C. A new parametrization of exchange–correlation generalized gradient approximation functionals. *The Journal of Chemical Physics* **2001**, *114*, 5497–5503.

(14) Peverati, R.; Zhao, Y.; Truhlar, D. G. Generalized Gradient Approximation That Recovers the Second-Order Density-Gradient Expansion with Optimized Across-the-Board Performance. *The Journal of Physical Chemistry Letters* **2011**, *2*, 1991–1997.

(15) Wilson, P. J.; Bradley, T. J.; Tozer, D. J. Hybrid exchange-correlation functional determined from thermochemical data and ab initio potentials. *The Journal of Chemical Physics* **2001**, *115*, 9233–9242.

(16) Boese, A. D.; Martin, J. M. L. Development of density functionals for thermochemical kinetics. *The Journal of Chemical Physics* **2004**, *121*, 3405–3416.

(17) Keal, T. W.; Tozer, D. J. Semiempirical hybrid functional with improved performance in an extensive chemical assessment. *The Journal of Chemical Physics* **2005**, *123*, 121103.

(18) Peverati, R.; Truhlar, D. G. Communication: A global hybrid generalized gradient approximation to the exchange-correlation functional that satisfies the second-order density-gradient constraint and has broad applicability in chemistry. *The Journal of Chemical Physics* **2011**, *135*, 191102.

(19) Chai, J.-D.; Head-Gordon, M. Systematic optimization of long-range corrected hybrid density functionals. *The Journal of Chemical Physics* **2008**, *128*, 084106.

(20) Chai, J.-D.; Head-Gordon, M. Long-range corrected hybrid density functionals with damped atom-atom dispersion corrections. *Phys. Chem. Chem. Phys.* **2008**, *10*, 6615–6620.

(21) Lin, Y.-S.; Li, G.-D.; Mao, S.-P.; Chai, J.-D. Long-Range Corrected Hybrid Density Functionals with Improved Dispersion Corrections. *Journal of Chemical Theory and Computation* **2013**, *9*, 263–272.

(22) Mardirossian, N.; Head-Gordon, M. ωB97X-V: A 10-parameter, range-separated hybrid, generalized gradient approximation density functional with nonlocal correlation, designed by a survival-of-the-fittest strategy. *Phys. Chem. Chem. Phys.* **2014**, *16*, 9904–9924.

(23) Peverati, R.; Truhlar, D. G. Exchange-Correlation Functional with Good Accuracy for Both Structural and Energetic Properties while Depending Only on the Density and Its Gradient. *Journal of Chemical Theory and Computation* **2012**, *8*, 2310–2319.

(24) Yu, H. S.; Zhang, W.; Verma, P.; He, X.; Truhlar, D. G. Nonseparable exchange-correlation functional for molecules, including homogeneous catalysis involving transition metals. *Phys. Chem. Chem. Phys.* **2015**, *17*, 12146–12160.

(25) Peverati, R.; Truhlar, D. G. Screened-exchange density functionals with broad accuracy for chemistry and solid-state physics. *Phys. Chem. Chem. Phys.* **2012**, *14*, 16187–16191.

(26) Boese, A. D.; Handy, N. C. New exchange-correlation density functionals: The role of the kinetic-energy density. *The Journal of Chemical Physics* **2002**, *116*, 9559–9569.

(27) Zhao, Y.; Truhlar, D. G. A new local density functional for main-group thermochemistry, transition metal bonding,

thermochemical kinetics, and noncovalent interactions. *The Journal of Chemical Physics* **2006**, *125*, 194101.

(28) Peverati, R.; Truhlar, D. G. M11-L: A Local Density Functional That Provides Improved Accuracy for Electronic Structure Calculations in Chemistry and Physics. *The Journal of Physical Chemistry Letters* **2012**, *3*, 117–124.

(29) Mardirossian, N.; Head-Gordon, M. Mapping the genome of meta-generalized gradient approximation density functionals: The search for B97M-V. *The Journal of Chemical Physics* **2015**, *142*, 074111.

(30) Zhao, Y.; Schultz, N. E.; Truhlar, D. G. Exchange-correlation functional with broad accuracy for metallic and nonmetallic compounds, kinetics, and noncovalent interactions. *The Journal of Chemical Physics* **2005**, *123*, 161103.

(31) Zhao, Y.; Schultz, N. E.; Truhlar, D. G. Design of Density Functionals by Combining the Method of Constraint Satisfaction with Parametrization for Thermochemistry, Thermochemical Kinetics, and Noncovalent Interactions. *Journal of Chemical Theory and Computation* **2006**, *2*, 364–382.

(32) Zhao, Y.; Truhlar, D. The M06 suite of density functionals for main group thermochemistry, thermochemical kinetics, noncovalent interactions, excited states, and transition elements: two new functionals and systematic testing of four M06-class functionals and 12 other functionals. *Theoretical Chemistry Accounts: Theory, Computation, and Modeling (Theoretica Chimica Acta)* **2008**, *120*, 215–241.

(33) Zhao, Y.; Truhlar, D. G. Density Functional for Spectroscopy: No Long-Range Self-Interaction Error, Good Performance for Rydberg and Charge-Transfer States, and Better Performance on Average than B3LYP for Ground States. *The Journal of Physical Chemistry A* **2006**, *110*, 13126–13130.

(34) Zhao, Y.; Truhlar, D. G. Exploring the Limit of Accuracy of the Global Hybrid Meta Density Functional for Main-Group Thermochemistry, Kinetics, and Noncovalent Interactions. *Journal of Chemical Theory and Computation* **2008**, *4*, 1849–1868.

(35) Peverati, R.; Truhlar, D. G. Improving the Accuracy of Hybrid Meta-GGA Density Functionals by Range Separation. *The Journal of Physical Chemistry Letters* **2011**, *2*, 2810–2817.

(36) Lin, Y.-S.; Tsai, C.-W.; Li, G.-D.; Chai, J.-D. Long-range corrected hybrid meta-generalized-gradient approximations with dispersion corrections. *The Journal of Chemical Physics* **2012**, *136*, 154109.

(37) Peverati, R.; Truhlar, D. G. An improved and broadly accurate local approximation to the exchange-correlation density functional: The MN12-L functional for electronic structure calculations in chemistry and physics. *Phys. Chem. Chem. Phys.* **2012**, *14*, 13171–13174.

(38) Yu, H. S.; He, X.; Truhlar, D. G. MN15-L: A New Local Exchange-Correlation Functional for Kohn–Sham Density Functional Theory with Broad Accuracy for Atoms, Molecules, and Solids. *Journal of Chemical Theory and Computation* **0**, *0*, null.

(39) Mardirossian, N.; Head-Gordon, M. Exploring the limit of accuracy for density functionals based on the generalized gradient approximation: Local, global hybrid, and range-separated hybrid functionals with and without dispersion corrections. *The Journal of Chemical Physics* **2014**, *140*, 18A527.

(40) Thom H. Dunning, J. Gaussian basis sets for use in correlated molecular calculations. I. The atoms boron through neon and hydrogen. *The Journal of Chemical Physics* **1989**, *90*, 1007–1023.

(41) Kendall, R. A.; Thom H. Dunning, J.; Harrison, R. J. Electron affinities of the first-row atoms revisited. Systematic basis sets and wave functions. *The Journal of Chemical Physics* **1992**, *96*, 6796–6806.

(42) Woon, D. E.; Thom H. Dunning, J. Gaussian basis sets for use in correlated molecular calculations. III. The atoms aluminum through argon. *The Journal of Chemical Physics* **1993**, *98*, 1358–1371.

(43) Jensen, F. Polarization consistent basis sets: Principles. *The Journal of Chemical Physics* **2001**, *115*, 9113–9125.

(44) Jensen, F. Polarization consistent basis sets. II. Estimating the Kohn–Sham basis set limit. *The Journal of Chemical Physics* **2002**, *116*, 7372–7379.

(45) Jensen, F. Polarization consistent basis sets. III. The importance of diffuse functions. *The Journal of Chemical Physics* **2002**, *117*, 9234–9240.

(46) Schäfer, A.; Horn, H.; Ahlrichs, R. Fully optimized contracted Gaussian basis sets for atoms Li to Kr. *The Journal of Chemical Physics* **1992**, *97*, 2571–2577.

(47) Schäfer, A.; Huber, C.; Ahlrichs, R. Fully optimized contracted Gaussian basis sets of triple zeta valence quality for atoms Li to Kr. *The Journal of Chemical Physics* **1994**, *100*, 5829–5835.

(48) Weigend, F.; Furche, F.; Ahlrichs, R. Gaussian basis sets of quadruple zeta valence quality for atoms H–Kr. *The Journal of Chemical Physics* **2003**, *119*, 12753–12762.

(49) Weigend, F.; Ahlrichs, R. Balanced basis sets of split valence, triple zeta valence and quadruple zeta valence quality for H to Rn: Design and assessment of accuracy. *Phys. Chem. Chem. Phys.* **2005**, *7*, 3297–3305.

(50) Rappoport, D.; Furche, F. Property-optimized Gaussian basis sets for molecular response calculations. *The Journal of Chemical Physics* **2010**, *133*, 134105.

(51) Gill, P. M.; Johnson, B. G.; Pople, J. A. A standard grid for density functional calculations. *Chemical Physics Letters* **1993**, *209*, 506 – 512.

(52) Chien, S.-H.; Gill, P. M. W. SG-0: A small standard grid for DFT quadrature on large systems. *Journal of Computational Chemistry* **2006**, *27*, 730–739.

(53) Shao, Y.; Gan, Z.; Epifanovsky, E.; Gilbert, A. T.; Wormit, M.; Kussmann, J.; Lange, A. W.; Behn, A.; Deng, J.; Feng, X. et al. Advances in molecular quantum chemistry contained in the Q-Chem 4 program package. *Molecular Physics* **2015**, *113*, 184–215.

(54) Řezáč, J.; Hobza, P. Describing Noncovalent Interactions beyond the Common Approximations: How Accurate Is the Gold Standard CCSD(T) at the Complete Basis Set Limit? *Journal of Chemical Theory and Computation* **2013**, *9*, 2151–2155.

(55) Mintz, B. J.; Parks, J. M. Benchmark Interaction Energies for Biologically Relevant Noncovalent Complexes Containing Divalent Sulfur. *The Journal of Physical Chemistry A* **2012**, *116*, 1086–1092.

(56) Řezáč, J.; Hobza, P. Advanced Corrections of Hydrogen Bonding and Dispersion for Semiempirical Quantum Mechanical Methods. *Journal of Chemical Theory and Computation* **2012**, *8*, 141–151.

(57) Faver, J. C.; Benson, M. L.; He, X.; Roberts, B. P.; Wang, B.; Marshall, M. S.; Kennedy, M. R.; Sherrill, C. D.; Merz, K. M. Formal Estimation of Errors in Computed Absolute Interaction Energies of Protein–Ligand Complexes. *Journal of Chemical Theory and Computation* **2011**, *7*, 790–797.

(58) Marshall, M. S.; Burns, L. A.; Sherrill, C. D. Basis set convergence of the coupled-cluster correction, $\delta_{MP2}^{CCSD(T)}$: Best practices for benchmarking noncovalent interactions and the attendant revision of the S22, NBC10, HBC6, and HSG databases. *The Journal of Chemical Physics* **2011**, *135*, 194102.

(59) Hohenstein, E. G.; Sherrill, C. D. Effects of Heteroatoms on Aromatic π–π Interactions: Benzene–Pyridine and Pyridine Dimer. *The Journal of Physical Chemistry A* **2009**, *113*, 878–886.

(60) Sherrill, C. D.; Takatani, T.; Hohenstein, E. G. An Assessment of Theoretical Methods for Nonbonded Interactions: Comparison to Complete Basis Set Limit Coupled-Cluster Potential Energy Curves for the Benzene Dimer, the Methane Dimer, Benzene–Methane, and Benzene–H_2S. *The Journal of Physical Chemistry A* **2009**, *113*, 10146–10159.

(61) Takatani, T.; David Sherrill, C. Performance of spin-component-scaled Møller-Plesset theory (SCS-MP2) for potential energy curves of noncovalent interactions. *Phys. Chem. Chem. Phys.* **2007**, *9*, 6106–6114.

(62) Jurečka, P.; Šponer, J.; Černý, J.; Hobza, P. Benchmark database of accurate (MP2 and CCSD(T) complete basis set limit) interaction energies of small model complexes, DNA base pairs, and amino acid pairs. *Phys. Chem. Chem. Phys.* **2006**, *8*, 1985–1993.

(63) Řezáč, J.; Riley, K. E.; Hobza, P. Benchmark Calculations of Noncovalent Interactions of Halogenated Molecules. *Journal of Chemical Theory and Computation* **2012**, *8*, 4285–4292.

(64) Witte, J.; Goldey, M.; Neaton, J. B.; Head-Gordon, M. Beyond Energies: Geometries of Nonbonded Molecular Complexes as Metrics for Assessing Electronic Structure Approaches. *Journal of Chemical Theory and Computation* **2015**, *11*, 1481–1492.

(65) Crittenden, D. L. A Systematic CCSD(T) Study of Long-Range and Noncovalent Interactions between Benzene and a Series of First- and Second-Row Hydrides and Rare Gas Atoms. *The Journal of Physical Chemistry A* **2009**, *113*, 1663–1669.

(66) Copeland, K. L.; Tschumper, G. S. Hydrocarbon/Water Interactions: Encouraging Energetics and Structures from DFT but Disconcerting Discrepancies for Hessian Indices. *Journal of Chemical Theory and Computation* **2012**, *8*, 1646–1656.

(67) Smith, D. G. A.; Jankowski, P.; Slawik, M.; Witek, H. A.; Patkowski, K. Basis Set Convergence of the Post-CCSD(T) Contribution to Noncovalent Interaction Energies. *Journal of Chemical Theory and Computation* **2014**, *10*, 3140–3150.

(68) Řezáč, J.; Riley, K. E.; Hobza, P. S66: A Well-balanced Database of Benchmark Interaction Energies Relevant to Biomolecular Structures. *Journal of Chemical Theory and Computation* **2011**, *7*, 2427–2438.

(69) Řezáč, J.; Riley, K. E.; Hobza, P. Extensions of the S66 Data Set: More Accurate Interaction Energies and Angular-Displaced Nonequilibrium Geometries. *Journal of Chemical Theory and Computation* **2011**, *7*, 3466–3470.

(70) Řezáč, J.; Huang, Y.; Hobza, P.; Beran, G. J. O. Benchmark Calculations

of Three-Body Intermolecular Interactions and the Performance of Low-Cost Electronic Structure Methods. *Journal of Chemical Theory and Computation* **2015**, *11*, 3065–3079.

(71) Granatier, J.; Pitoňák, M.; Hobza, P. Accuracy of Several Wave Function and Density Functional Theory Methods for Description of Noncovalent Interaction of Saturated and Unsaturated Hydrocarbon Dimers. *Journal of Chemical Theory and Computation* **2012**, *8*, 2282–2292.

(72) Li, S.; Smith, D. G. A.; Patkowski, K. An accurate benchmark description of the interactions between carbon dioxide and polyheterocyclic aromatic compounds containing nitrogen. *Phys. Chem. Chem. Phys.* **2015**, *17*, 16560–16574.

(73) Boese, A. D. Assessment of Coupled Cluster Theory and more Approximate Methods for Hydrogen Bonded Systems. *Journal of Chemical Theory and Computation* **2013**, *9*, 4403–4413.

(74) Boese, A. D. Basis set limit coupled-cluster studies of hydrogen-bonded systems. *Molecular Physics* **2015**, *113*, 1618–1629.

(75) Boese, A. D. Density Functional Theory and Hydrogen Bonds: Are We There Yet? *ChemPhysChem* **2015**, *16*, 978–985.

(76) Lao, K. U.; Schäffer, R.; Jansen, G.; Herbert, J. M. Accurate Description of Intermolecular Interactions Involving Ions Using Symmetry-Adapted Perturbation Theory. *Journal of Chemical Theory and Computation* **2015**, *11*, 2473–2486.

(77) Lao, K. U.; Herbert, J. M. An improved treatment of empirical dispersion and a many-body energy decomposition scheme for the explicit polarization plus symmetry-adapted perturbation theory (XSAPT) method. *The Journal of Chemical Physics* **2013**, *139*, 034107.

(78) Lao, K. U.; Herbert, J. M. Accurate and Efficient Quantum Chemistry Calculations for Noncovalent Interactions in Many-Body Systems: The XSAPT Family of Methods. *The Journal of Physical Chemistry A* **2015**, *119*, 235–252.

(79) Temelso, B.; Archer, K. A.; Shields, G. C. Benchmark Structures and Binding Energies of Small Water Clusters with Anharmonicity Corrections. *The Journal of Physical Chemistry A* **2011**, *115*, 12034–12046.

(80) Mardirossian, N.; Lambrecht, D. S.; McCaslin, L.; Xantheas, S. S.; Head-Gordon, M. The Performance of Density Functionals for Sulfate–Water Clusters. *Journal of Chemical Theory and Computation* **2013**, *9*, 1368–1380.

(81) Bryantsev, V. S.; Diallo, M. S.; van Duin, A. C. T.; Goddard, W. A. Evaluation of B3LYP, X3LYP, and M06-Class Density Functionals for Predicting the Binding Energies of Neutral, Protonated, and Deprotonated Water Clusters. *Journal of Chemical Theory and Computation* **2009**, *5*, 1016–1026.

(82) Goerigk, L.; Grimme, S. A General Database for Main Group Thermochemistry, Kinetics, and Noncovalent Interactions – Assessment of Common and Reparameterized (meta-)GGA Density Functionals. *Journal of Chemical Theory and Computation* **2010**, *6*, 107–126.

(83) Karton, A.; O'Reilly, R. J.; Chan, B.; Radom, L. Determination of Barrier Heights for Proton Exchange in Small Water, Ammonia, and Hydrogen Fluoride Clusters with G4(MP2)-Type, MPn, and SCS-MPn Procedures–A Caveat. *Journal of Chemical Theory and Computation* **2012**, *8*, 3128–3136.

(84) Chan, B.; Gilbert, A. T. B.; Gill, P. M. W.; Radom, L. Performance of Density Functional Theory Procedures for

the Calculation of Proton-Exchange Barriers: Unusual Behavior of M06-Type Functionals. *Journal of Chemical Theory and Computation* **2014**, *10*, 3777–3783.

(85) Fanourgakis, G. S.; Aprà, E.; Xantheas, S. S. High-level ab initio calculations for the four low-lying families of minima of $(H_2O)_{20}$. I. Estimates of MP2/CBS binding energies and comparison with empirical potentials. *The Journal of Chemical Physics* **2004**, *121*, 2655–2663.

(86) Anacker, T.; Friedrich, J. New accurate benchmark energies for large water clusters: DFT is better than expected. *J. Comput. Chem.* **2014**, *35*, 634–643.

(87) Tentscher, P. R.; Arey, J. S. Binding in Radical-Solvent Binary Complexes: Benchmark Energies and Performance of Approximate Methods. *Journal of Chemical Theory and Computation* **2013**, *9*, 1568–1579.

(88) Kozuch, S.; Martin, J. M. L. Halogen Bonds: Benchmarks and Theoretical Analysis. *Journal of Chemical Theory and Computation* **2013**, *9*, 1918–1931.

(89) Bauzá, A.; Alkorta, I.; Frontera, A.; Elguero, J. On the Reliability of Pure and Hybrid DFT Methods for the Evaluation of Halogen, Chalcogen, and Pnicogen Bonds Involving Anionic and Neutral Electron Donors. *Journal of Chemical Theory and Computation* **2013**, *9*, 5201–5210.

(90) de-la Roza, A. O.; Johnson, E. R.; DiLabio, G. A. Halogen Bonding from Dispersion-Corrected Density-Functional Theory: The Role of Delocalization Error. *Journal of Chemical Theory and Computation* **2014**, *10*, 5436–5447.

(91) Steinmann, S. N.; Piemontesi, C.; Delachat, A.; Corminboeuf, C. Why are the Interaction Energies of Charge-Transfer Complexes Challenging for DFT? *Journal of Chemical Theory and Computation* **2012**, *8*, 1629–1640.

(92) Karton, A.; Gruzman, D.; Martin, J. M. L. Benchmark Thermochemistry of the C_nH_{2n+2} Alkane Isomers (n = 2–8) and Performance of DFT and Composite Ab Initio Methods for Dispersion-Driven Isomeric Equilibria. *The Journal of Physical Chemistry A* **2009**, *113*, 8434–8447.

(93) Kozuch, S.; Bachrach, S. M.; Martin, J. M. Conformational Equilibria in Butane-1,4-diol: A Benchmark of a Prototypical System with Strong Intramolecular H-bonds. *The Journal of Physical Chemistry A* **2014**, *118*, 293–303.

(94) Gruzman, D.; Karton, A.; Martin, J. M. L. Performance of Ab Initio and Density Functional Methods for Conformational Equilibria of C_nH_{2n+2} Alkane Isomers (n = 4–8). *The Journal of Physical Chemistry A* **2009**, *113*, 11974–11983.

(95) Wilke, J. J.; Lind, M. C.; Schaefer, H. F.; Csaszar, A. G.; Allen, W. D. Conformers of Gaseous Cysteine. *Journal of Chemical Theory and Computation* **2009**, *5*, 1511–1523.

(96) Martin, J. M. L. What Can We Learn about Dispersion from the Conformer Surface of n-Pentane? *The Journal of Physical Chemistry A* **2013**, *117*, 3118–3132.

(97) Yoo, S.; Aprà, E.; Zeng, X. C.; Xantheas, S. S. High-Level Ab Initio Electronic Structure Calculations of Water Clusters $(H_2O)_{16}$ and $(H_2O)_{17}$: A New Global Minimum for $(H_2O)_{16}$. *The Journal of Physical Chemistry Letters* **2010**, *1*, 3122–3127.

(98) Fogueri, U. R.; Kozuch, S.; Karton, A.; Martin, J. M. The Melatonin Conformer Space: Benchmark and Assessment of Wave Function and DFT Methods for a

Paradigmatic Biological and Pharmacological Molecule. *The Journal of Physical Chemistry A* **2013**, *117*, 2269–2277.

(99) Kesharwani, M. K.; Karton, A.; Martin, J. M. L. Benchmark ab Initio Conformational Energies for the Proteinogenic Amino Acids through Explicitly Correlated Methods. Assessment of Density Functional Methods. *Journal of Chemical Theory and Computation* **2016**, *12*, 444–454.

(100) Yu, L.-J.; Sarrami, F.; Karton, A.; O'Reilly, R. J. An assessment of theoretical procedures for π-conjugation stabilisation energies in enones. *Molecular Physics* **2015**, *113*, 1284–1296.

(101) Karton, A.; Martin, J. M. Explicitly correlated benchmark calculations on C_8H_8 isomer energy separations: how accurate are DFT, double-hybrid, and composite ab initio procedures? *Molecular Physics* **2012**, *110*, 2477–2491.

(102) Yu, L.-J.; Karton, A. Assessment of theoretical procedures for a diverse set of isomerization reactions involving double-bond migration in conjugated dienes. *Chemical Physics* **2014**, *441*, 166 – 177.

(103) Karton, A.; Daon, S.; Martin, J. M. W4-11: A high-confidence benchmark dataset for computational thermochemistry derived from first-principles W4 data. *Chemical Physics Letters* **2011**, *510*, 165 – 178.

(104) Manna, D.; Martin, J. M. L. What Are the Ground State Structures of C_{20} and C_{24}? An Explicitly Correlated Ab Initio Approach. *The Journal of Physical Chemistry A* **2016**, *120*, 153–160.

(105) Curtiss, L. A.; Raghavachari, K.; Trucks, G. W.; Pople, J. A. Gaussian-2 theory for molecular energies of first- and second-row compounds. *The Journal of Chemical Physics* **1991**, *94*, 7221–7230.

(106) Zhao, Y.; González-García, N.; Truhlar, D. G. Benchmark Database of Barrier Heights for Heavy Atom Transfer, Nucleophilic Substitution, Association, and Unimolecular Reactions and Its Use to Test Theoretical Methods. *The Journal of Physical Chemistry A* **2005**, *109*, 2012–2018.

(107) Zhao, Y.; Lynch, B. J.; Truhlar, D. G. Multi-coefficient extrapolated density functional theory for thermochemistry and thermochemical kinetics. *Phys. Chem. Chem. Phys.* **2005**, *7*, 43–52.

(108) Lynch, B. J.; Zhao, Y.; Truhlar, D. G. Effectiveness of Diffuse Basis Functions for Calculating Relative Energies by Density Functional Theory. *The Journal of Physical Chemistry A* **2003**, *107*, 1384–1388.

(109) Grimme, S.; Kruse, H.; Goerigk, L.; Erker, G. The Mechanism of Dihydrogen Activation by Frustrated Lewis Pairs Revisited. *Angewandte Chemie International Edition* **2010**, *49*, 1402–1405.

(110) Goerigk, L.; Grimme, S. Efficient and Accurate Double-Hybrid-Meta-GGA Density Functionals–Evaluation with the Extended GMTKN30 Database for General Main Group Thermochemistry, Kinetics, and Noncovalent Interactions. *Journal of Chemical Theory and Computation* **2011**, *7*, 291–309.

(111) Krieg, H.; Grimme, S. Thermochemical benchmarking of hydrocarbon bond separation reaction energies: Jacob's ladder is not reversed! *Molecular Physics* **2010**, *108*, 2655–2666.

(112) O'Reilly, R. J.; Karton, A. A dataset of highly accurate homolytic N–Br bond dissociation energies obtained by Means of W2 theory. *International Journal of Quantum Chemistry* **2016**, *116*, 52–60.

(113) Karton, A.; O'Reilly, R. J.; Radom, L. Assessment of Theoretical Procedures for

Calculating Barrier Heights for a Diverse Set of Water-Catalyzed Proton-Transfer Reactions. *The Journal of Physical Chemistry A* **2012**, *116*, 4211–4221.

(114) Karton, A.; Schreiner, P. R.; Martin, J. M. L. Heats of formation of platonic hydrocarbon cages by means of high-level thermochemical procedures. *Journal of Computational Chemistry* **2016**, *37*, 49–58.

(115) Karton, A.; Goerigk, L. Accurate reaction barrier heights of pericyclic reactions: Surprisingly large deviations for the CBS-QB3 composite method and their consequences in DFT benchmark studies. *Journal of Computational Chemistry* **2015**, *36*, 622–632.

(116) Yu, L.-J.; Sarrami, F.; O'Reilly, R. J.; Karton, A. Reaction barrier heights for cycloreversion of heterocyclic rings: An Achilles' heel for DFT and standard ab initio procedures. *Chemical Physics* **2015**, *458*, 1 – 8.

(117) Zheng, J.; Zhao, Y.; Truhlar, D. G. Representative Benchmark Suites for Barrier Heights of Diverse Reaction Types and Assessment of Electronic Structure Methods for Thermochemical Kinetics. *Journal of Chemical Theory and Computation* **2007**, *3*, 569–582.

(118) Karton, A.; Tarnopolsky, A.; Lamère, J.-F.; Schatz, G. C.; Martin, J. M. L. Highly Accurate First-Principles Benchmark Data Sets for the Parametrization and Validation of Density Functional and Other Approximate Methods. Derivation of a Robust, Generally Applicable, Double-Hybrid Functional for Thermochemistry and Thermochemical Kinetics. *The Journal of Physical Chemistry A* **2008**, *112*, 12868–12886.

(119) Yu, L.-J.; Sarrami, F.; O'Reilly, R. J.; Karton, A. Can DFT and ab initio methods describe all aspects of the potential energy surface of cycloreversion reactions? *Molecular Physics* **2016**, *114*, 21–33.

(120) Chakravorty, S. J.; Gwaltney, S. R.; Davidson, E. R.; Parpia, F. A.; Fischer, C. F. Ground-state correlation energies for atomic ions with 3 to 18 electrons. *Phys. Rev. A* **1993**, *47*, 3649–3670.

(121) Tang, K. T.; Toennies, J. P. The van der Waals potentials between all the rare gas atoms from He to Rn. *The Journal of Chemical Physics* **2003**, *118*, 4976–4983.

(122) Becke, A. D. Density functional calculations of molecular bond energies. *The Journal of Chemical Physics* **1986**, *84*, 4524–4529.

(123) Ceperley, D. M.; Alder, B. J. Ground State of the Electron Gas by a Stochastic Method. *Phys. Rev. Lett.* **1980**, *45*, 566–569.

(124) Perdew, J. P.; Wang, Y. Accurate and simple analytic representation of the electron-gas correlation energy. *Phys. Rev. B* **1992**, *45*, 13244–13249.

(125) Vosko, S. H.; Wilk, L.; Nusair, M. Accurate spin-dependent electron liquid correlation energies for local spin density calculations: a critical analysis. *Can. J. Phys.* **1980**, *58*, 1200–1211.

(126) Stoll, H.; Golka, E.; Preuß, H. Correlation energies in the spin-density functional formalism. *Theoretical Chemistry Accounts: Theory, Computation, and Modeling (Theoretica Chimica Acta)* **1980**, *55*, 29–41.

(127) Grafenstein, J.; Izotov, D.; Cremer, D. Avoiding singularity problems associated with meta-GGA (generalized gradient approximation) exchange and correlation functionals containing the kinetic energy density. *The Journal of Chemical Physics* **2007**, *127*, 214103.

(128) Johnson, E. R.; Becke, A. D.; Sherrill, C. D.; DiLabio, G. A. Oscillations in meta-generalized-gradient approximation potential energy surfaces for dispersion-bound complexes. *The Journal of Chemical Physics* **2009**, *131*, 034111.

(129) Wheeler, S. E.; Houk, K. N. Integration Grid Errors for Meta-GGA-Predicted Reaction Energies: Origin of Grid Errors for the M06 Suite of Functionals. *Journal of Chemical Theory and Computation* **2010**, *6*, 395–404.